Doctoral Thesis

# Inclusive Bottom Production in $p\bar{p}$ Collisions at $\sqrt{s} = 1.8$ TeV at DØ Central Detector Region

Vitor Oguri

Centro Brasileiro de Pesquisas Físicas
(CBPF)

Rio de Janeiro — August, 1995

# Acknowledgements

To my advisor and friend Professor Alberto Santoro for his guidance, for his contagious enthusiasm, for the constant incentive and for the trust he has deposited on me. I also thank him for having provided me with the basic conditions to perform this work.

To all the members of the DØ International Collaboration, that directly, or indirectly, have contributed to the realization of my thesis work. In particular, to Alberto Santoro, Moacyr de Souza, Arthur Maciel, Gilvan Alves and Guilherme Lima, from LAFEX/CBPF, to Kamel Bazizi and Thorstein Huehn (University of California, Riverside) and to all of those with whom I have the pleasure to collaborate directly during the two and a half years period that I have been with the Fermilab. Specially, I thank also the leaders of the B Physics Group of the Collaboration, Dan Green, Dave Hedin and Andrej Zieminski, for their constant critics and suggestions, for the incentive and excellent atmosphere for scientific discussions that I have found in all the meetings of the Group. To my colleagues Mike Fortner, John Butler, Tom Diehl, Kamel Bazizi, Ken Johns and Mary Ann Cummings, that were responsible for various of the specific tasks that I have participated since my arrival at the Fermilab and for everything that I have learned from them. To my shift colleagues, Chris Murphy, Cecilia Gerber, John Balderston, Dave Fein and Guilherme Lima for the discussions on physics at the most oddest occasions and locations.

To Paul Grannis, Gene Fisk, Jeff Appel and Roy Rubinstein, for the encouragement and invaluable support that they have given me, without which my stay at the Fermilab wouldn't be as pleasant and fruitful as it was.

To my friend Francisco Caruso, a great supporter, for having created in the UERJ (Rio de Janeiro State University) the Department of Nuclear Physics and High Energies (DFNAE) and its High Energy Physics Group, that I have joined since its beginning. To him I leave my gratitude for the support he has granted me during all the time he was in charge of the DFNAE. I can't help thanking as well the support I have received from the Direction of the Physics Institute, through Professor José Ricardo de Arruda and Professor Nádia Lima Caruso, and from the Vice-Chancellors of Graduation and Research of UERJ - at distinct occasions - Professors Reinaldo Guimarães and Roberto Bezerra. To all my colleagues in UERJ that had helped me in many different ways during the elaboration of the thesis, specially to Arnaldo Santiago, Gerson Pech, Mordka Szajnberg, José de Sá Borges and Pedro Von Ranke.

To my LAFEX colleagues and to Myriam Simões Coutinho, from CFC, for the atmosphere of friendship that I have found in the CBPF.

To my family for the understanding, supporting and motivation that they have always given me, even in the most difficult moments of this journey, I have no words for thanking them. To my parents for all the incentive that I have always received from them throughout my whole life.

Last but not least, my institutional acknowledgements: to UERJ, for releasing me during the period I was staying abroad, to FERMILAB for the support I have received and to CBPF for the great conditions that have allowed me to conclude my analysis and write this thesis.

**Abstract**

The inclusive $b$-quark cross section at center of mass energy of 1.8 TeV, at the Fermilab Tevatron $p\bar{p}$ Collider, is determined from the inclusive muon cross section, with data taken during 1992-1993 at DØ detector.

The analyses were realized in the detector central region. The global efficiency components were estimated from the pseudo-random event generator ISAJET, from cosmic ray data and from DØ muon data itself.

The $b$-quark cross section seems to be well described by next to leading order (NLO) QCD prediction for the rapidity $|y| < 1.0$ and transverse momentum greater than 6.0 GeV kinematical region.

# Contents

# List of Figures

# List of Tables

# Chapter 1

# Introduction

The main purpose of this thesis is the determination of the $b$-quark (*bottom*) production cross section in proton-antiproton ($p\bar{p}$) collisions at $\sqrt{s} =$ 1.8 TeV of energy in the center of mass of the proton-antiproton system, at a wide spectrum of transverse momentum ($p_T$), *i.e.*, $6.0 \leq p_T \leq 40.0$ GeV. The original result of this thesis contributes significantly to the study of heavy quarks production, one of the most recent focus of attention in the area of high energy experimental physics. In particular, the result achieved herein was utilized by the DØ collaboration to establish some of the criteria for the selection of events in the identification of the $t$-quark (*top*).

With the discovery of the $t$-quark in the beginning of this year [1, 2], we can to synthetize the knowledge established by the high-energy physics by stating that the elementary particles of Nature - that constitute all the matter of the Universe - are spin 1/2 fermions that can be grouped in six pairs of **quarks** and **leptons** varieties (table 1.1) and spin 1 bosons (table

1.2) associated to the fundamental interactions among particles.

| | | | | |
|---|---|---|---|---|
| quarks($q$) | up($u$) | charm($c$) | top($t$) | electric charge 2/3 |
| | down($d$) | strange($s$) | bottom($b$) | $-1/3$ |
| leptons($l$) | $e$-neutrino($\nu_e$) | $\mu$-neutrino($\nu_\mu$) | $\tau$-neutrino($\nu_\tau$) | 0 |
| | electron($e$) | muon($\mu$) | tau($\tau$) | $-1$ |

Table 1.1: Fundamental Particles.

The associated antiparticles are generally represented by $\bar{q}$ ($\bar{u}, \bar{d}, \bar{c}, \bar{s}, \bar{t}, \bar{b}$) in the case of quarks and neutrinos ($\bar{\nu}_e, \bar{\nu}_\mu, \bar{\nu}_\tau$), and by $l^+$ ($e^+, \mu^+, \tau^+$) in the case of charged leptons.

Quarks and leptons may interact by exchanging spin 1 bosons (table 1.2), in either the **electromagnetic** or **weak** modes. Besides that, the quarks have an additional level of freedom (**color**) that is responsible for the **strong** interactions between them.

| **interactions** | bosons mediators | mass (GeV) | electric charge |
|---|---|---|---|
| **strong** | gluon ($g$) | 0 | 0 |
| **electromagnetic** | photon ($\gamma$) | 0 | 0 |
| **weak** | $W^\pm$ | 80 | $\pm1$ |
| | $Z$ | 91 | 0 |

Table 1.2: Bosons mediators of the fundamental interactions.

While leptons can be directly detected, the quarks are found confined to the matter in a combination between them that constitutes the **hadrons**.

At a later scale, the hadrons combine themselves to form nucleons that, together with the leptons electrons, constitute the **atoms**.

These, on their turn, form the **molecules** that constitute all the existing substances and complex systems, such as planets.

When the level of complexity is such that the mass becomes "big", the gravitational interaction - believed to be mediated by a spin 2 boson (*graviton*) - becomes important, or even dominating, and starts to determine a certain type of behavior or evolution of systems such as planets, star and galaxies.

In the composition of the quarks, the hadrons are divided in two statistical classes (table 1.3):

- **mesons** – bosons constituted of pairs of quark-antiquark ($q\bar{q}$).
- **barions** – fermions constituted of three types of quarks ($qqq$).

The $u$, $d$ and $s$ quarks, that constitute the most abundant hadrons such as the protons, neutrons, pions and kaons, are called the light quarks, once their "constituent massess" are smaller than that of the proton ($m_p \approx 1$ GeV). The $c$, $t$ and $b$ quarks, that constitute the hadrons with very short lifetime ($\approx 10^{-12}$s), are commonly known as heavy quarks[1], as their "constituent masses" are greater than that of the proton.

[1] The $c$-quark is in the borderline of the heavy quarks classification.

| hadrons | | composition | electric charge |
|---|---|---|---|
| mesons | pion ($\pi^-$) | $d\bar{u}$ | -1 |
| | kaon ($K^-$) | $s\bar{u}$ | -1 |
| | J/$\psi$ | $c\bar{c}$ | 0 |
| barions | proton ($p$) | $uud$ | 1 |
| | neutron ($n$) | $udd$ | 0 |

Table 1.3: Composition of some typical hadrons.

In the $q\bar{q}$ and $qqq$ configurations, *i.e.*, when they constitute the hadrons, the quarks are generically known as valence quarks[2]. Besides these valence quarks, there is also in the hadron the continuous creation of a cloud of gluons and pairs of virtual $q\bar{q}$, that have an important role in the high-energy hadrons collisions.

High-energy collisions may annihilate a hadron and, by this way, experimental evidence about the quarks are obtained and studied. At another end, high-energy collisions between leptons can also generate quarks and these ones materialize into hadrons. In any of such cases, some hadrons decay into leptons and, through correlations between these leptons and other resulting hadrons, quantitative information concerning the generating or producing process of quarks, or even regarding the hadrons structure, are obtained.

[2]In analogy to the electrons that constitute the atoms.

- **The Tevatron**

Groups of protons circulating clockwise and antiprotons circulating anti-clockwise, at the energy of 900 GeV for each group, in a period of 20 $\mu$s, constitute the $p\bar{p}$ beam of the Tevatron (figure 1.1) at the Fermilab[3].

This process begins in the pre-accelerator, where hydrogen ions are accelerated in a pulse mode, at frequency of 15 Hz, up to energies of 750 keV, by a Cockroft-Walton type electric potential multiplier system. Next, the ions beam is injected in a linear accelerator (LINAC), with 150 m of length, where electric fields generated in the radio frequencies region (RF) transmit energies of 200 MeV to the ions ("Run 1A"). Then, the electrons are removed and the protons are grouped into small bunches.

In a small synchrotron[4] accelerator, with 150 m of length, called *Booster*, the protons are accelerated at an energy of 8 GeV.

After this initial process, the protons are injected into the Main Ring of the accelerator, which is a large synchrotron of approximately 1 km of radius, that utilizes conventional electro-magnets, and can be accelerated up to the energy of 150 GeV.

Once inside the main ring, at a first stage, protons at an energy of 120 GeV are extracted and collide with a fixed nickel (Ni) target, for the production of anti-protons. These are kept inside an accumulator until a sufficient quantity

[3]Fermi National Accelerator Laboratory in Batavia, Illinois, USA.

[4]Mode by which charged particles are kept in their path by magnetic fields generated by large electro-magnets and accelerated by electric fields in the RF band.

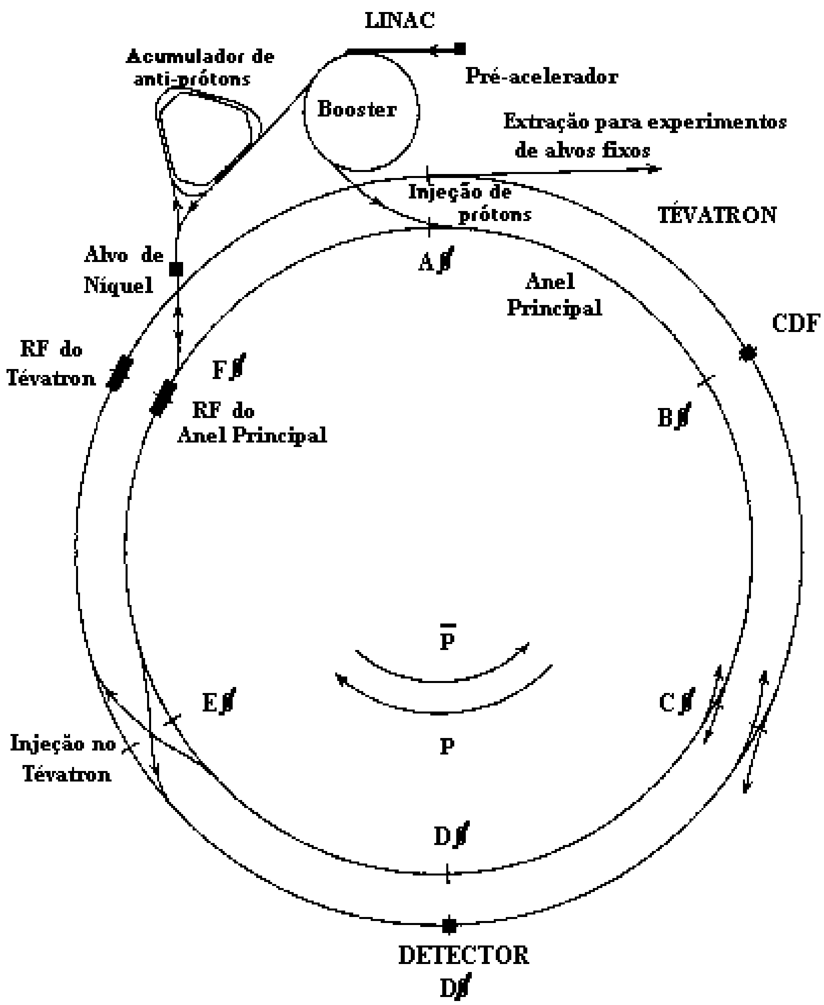


Figure 1.1: Fermilab Tevatron Scheme.

is stored and then, they are re-injected into the main ring in an opposite direction to the protons movement.

When the energy of the protons and antiprotons is in the range of 150 GeV, both beams are properly injected into the Tevatron, which is also a synchrotron collision ring, slightly below the main ring, in which electro-magnets that generate magnetic fields are made of super-conductivity materials.

In figure 1.1, the two beam intersection zones can be seen;

**DØ** – where the DØ detector is located

**BØ** – where the other large detector (CDF) of the Fermilab is located

• **Summary**

The data used in this thesis originates from the first year (1992 - 1993) of operation ("run 1A") of the DØ detector [3], built by the so called DØ collaboration[5], located in the $p\bar{p}$ (*proton-antiproton*) collider circular tunnel in the **Tevatron** of the Fermilab.

Due to the total high energy of the beam established in the Tevatron, in relation to the center of mass ($\sqrt{s} = 1.8$ TeV) of the proton-antiproton system, cross sections with reasonable values for the production of heavy quarks are expected and, therefore, a significant quantity of $b\bar{b}$ pairs (bottom-antibottom) are produced. In a much smaller scale, $t\bar{t}$ pairs (*top-antitop*), recently observed [1, 2], are also produced.

The main result of this thesis is the determination of the $b$-quark production cross section, through the detection of the muons ($\mu$) resulting from the decay of several hadrons generated after the inelastic $p\bar{p}$ collisions. This result, is part of the efforts of the study group of the DØ collaboration related to the bottom physics in hadronic collisions, that involves the $b$-quark production, the determination of the quarks and gluons distribution in the proton, the hadronization of quarks in mesons and barions and the decay of these ones into leptons.

A summary of the analysis of this result, for which I have worked for some years, was published this year (1995) in the form of an article [4] from the

[5]See Appendix A for the list of collaborators and institutions.

DØ collaboration, with the title "*Inclusive $\mu$ and b-Quark Production Cross Section in $p\bar{p}$ Collision at $\sqrt{s} = 1.8$ TeV*", in "*Physical Review Letters*".

Throughout all this work, with the exception of some explicit cases, the natural units system is used, as commonly adopted in the high-energy physics, where the light speed in the vacuum ($c$) is taken as a speed unit and all the figures that have action dimensions, are measured in units of the reduced Plank constant ($\hbar$). Indicating

$$c = \hbar = 1$$

all the other figures are expressed in multiples of the energy unit in electron-volt ($eV$).

Following this initial chapter, chapter 2 describes the various mechanisms of $b\bar{b}$ production, which occurs in an inelastic $p\bar{p}$ collision, and also presents the figures and parameters necessary for the determination of the $b$-quark production cross section.

The chapter 3 is constituted of a brief description of the DØ detector and of the author's direct contribution in the construction, maintenance and implementation of the detector, as a member of the DØ collaboration, associated with the "Laboratório de Cosmologia e Física Experimental de Altas Energias (LAFEX)", of the "Centro Brasileiro de Pesquisas Físicas (CBPF)", since 1991. Besides this, it contains also a description of the processes for the data acquisition, for the events selection (*trigger*), and for the software packages utilized by all the members of the collaboration in the simulation and reconstruction of the events.

In chapter 4, besides the initial criteria of selection and quality of the data used in the analysis, it is also presented the procedures and the determination of the global efficiency in the detection of muons and the main results of the thesis: the inclusive muons and $b$-quarks production cross section.

Finally, in chapter 5, the conclusions and perspectives of this work are presented.

# Chapter 2

# Bottom Production

One of the adequate channels (forms of occurrence) for the search of events that indicate the production of heavy quarks in a $p\bar{p}$ collision, is the one in which the final states involve the presence of leptons and hadronic jets with momentum components in the transversal plane to the $p\bar{p}$ beam in the range of some GeV ($\sim$ 10 GeV).

As an example, the process

$$p\bar{p} \rightarrow \mu + jets$$

is subjacent to various processes that involve the $b$-quark production.

Since the first observations of hadronic jets originated from $p\bar{p}$ collisions, in 1982, by the UA2 collaboration [5] at the CERN[1], the ratio estimated by the strong interactions theory[2] and the subsequent leptons spectrum[3] predicted by the V - A theory[6, 7, 8, 9, 10], generally, have been satisfactorily

[1]European Laboratory for Particle Physics, Genebra, Switzerland.
[2]Cromodinâmica Quântica (QCD).
[3]Due to the weak decays.

confirmed, which establishes, in a certain way, the applicability of such theories to the semi-leptonic and hadronic processes induced in a $p\bar{p}$ collision.

## 2.1 Parton Model

The scheme shown in figure 2.1, which is based the majority of the descriptions and simulations of events in a hadronic collision, illustrates some of the processes that constitute a $p\bar{p}$ inelastic collision, following the **Parton Model** of Feynman [11, 12], *i.e.*:

- the hadrons that will collide are constituted by quarks ($q$), antiquarks ($\bar{q}$) and by almost free gluons ($g$) (also called partons).

- the non-elementary nature of a hadron is characterized by $f_i(x)$ functions, that describe the partons distribution (of $i$-type) with fraction $x$ of the total quadri-momentum of the hadron.

- the heavy quarks production ($Q$ or $\bar{Q}$) occurs due to strong interactions between the punctual constituents of the hadrons (partons).

- the final states are the ones known as jets (hadronic) of mesons or barions, that are characterized by the $D_Q^h(z)$ probabilities of occurrence (known as fragmentation functions) of a hadron $h$ with fraction $z$ of the energy-momentum of the heavy quark $Q$ that produced it.

Due to the presence of hadronic jets and/or due to its subsequent weak interaction decays, *i.e.*, due also to the presence of leptons with $p_T$ values in the GeV range, the $b$-quark production can be reconstructed.

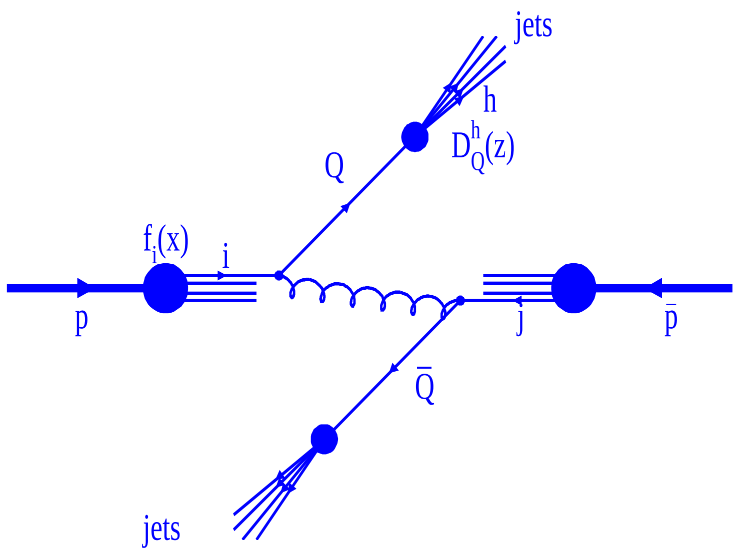


Figure 2.1: Inelastic $p\bar{p}$ collision in the Parton Model.

In accordance to the parton model, the cross section production ($\sigma_{Q\bar{Q}}$) of a pair of heavy $Q\bar{Q}$, originated from a $p\bar{p}$ collision, can be calculated as the sum of the cross sections in the elementary processes between partons (*hard scattering*), mediated by the respective distribution functions, as it is shown in the expression 2.1,

$$\sigma_{Q\bar{Q}} = \sum_{i,j} \int \int dx_1 \; dx_2 \; \hat{\sigma}_{ij}(x_1 x_2 s) \; f_i(x_1) f_j(x_2) \qquad (2.1)$$

where $\sqrt{s}$ is the energy of the $p\bar{p}$ system in relation to its center of mass, $\hat{\sigma}_{ij}$ is the cross section of the elementary process $ij \rightarrow Q\bar{Q}$, which effective energy is $\hat{s} = x_1 x_2 s$.

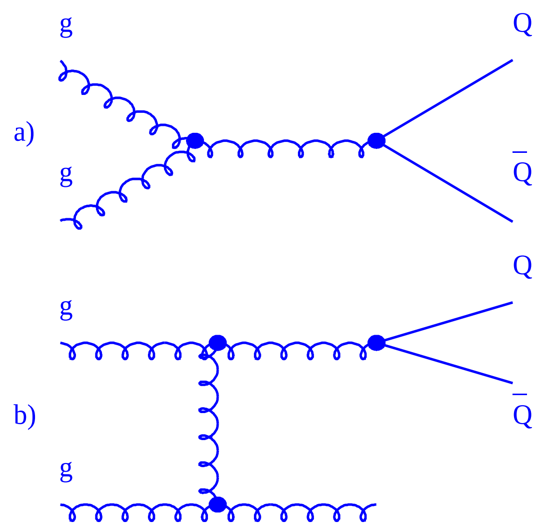


Figure 2.2: Samples of processes in $\alpha_s^2$ (a) and $\alpha_s^3$ (b).

The main mechanisms of heavy quark production, in the Tevatron, in terms of the strong coupling constant ($\alpha_s$), are:

- Order 2 processes ($\alpha_s^2$), usually dominating, such as the gluon fusion (Figure 2.2 a).
- High-order processes ($\alpha_s^3$), such as the fraction of gluons (Figure 2.2 b).

In any degree of approximation of a scattering process, secondary processes of radiation and creation of particle-antiparticle virtual pairs lead to corrections of several pre-defined quantities, such as the mass or the strong coupling constant.

- **The Strong Coupling Constant**

In the case of a scattering caused by strong interactions, the available calculations [13, 14, 15] of the cross section utilize the coupling constant $\alpha_s$ in two subsequent approximations, LO (*Leading Order*) and NLO (*Next to Leading Order*).

In either the LO or NLO, in an elementary parton-parton process, the coupling constant $\alpha_s$ depends on the modulus of the square of the difference of the quadri-momenta of the colliding partons. This variable, known as invariant transferred quadri-momentum, is represented by $Q$. Usually, $\alpha_s$ is expressed in terms of a reference value $\Lambda$ for $Q$, which avoids the singularities associated with the secondary processes of gluon radiation and creation of quark-antiquark virtual pairs, *i.e.*:

$$\alpha_s(Q) = f(Q^2/\Lambda^2)$$

in such a way that $\alpha_s \to 0$, when $Q \gg \Lambda$, and this fact is the one that justifies the utilization of perturbative methods in the study of $p\bar{p}$ collisions inside the Tevatron.

The reference value for the transferred invariable quadri-momentum $Q$, also called $\Lambda_{QCD}$, depends on the variety of quarks admitted in the theory and lies within 100 and 250 MeV.

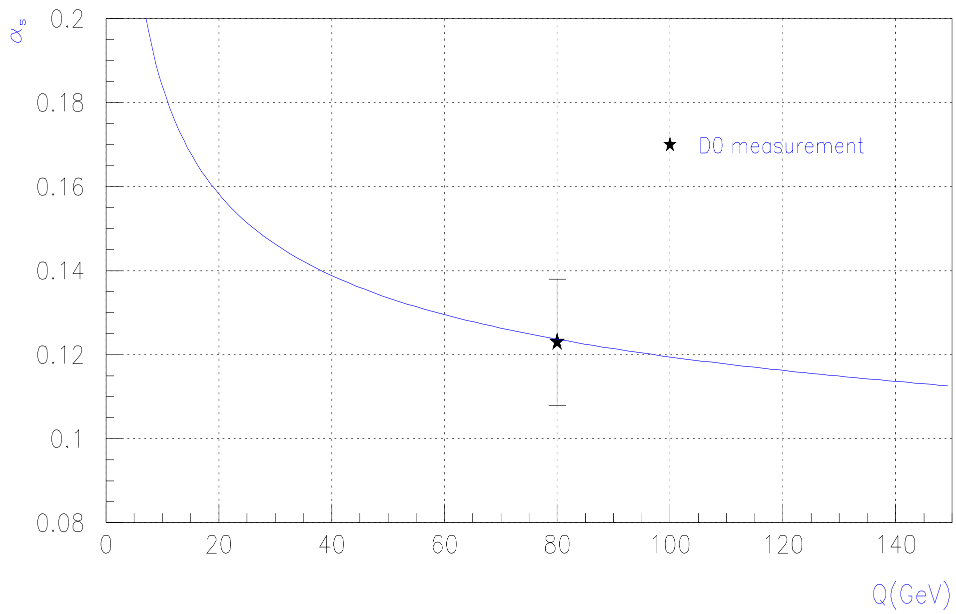


Figure 2.3: Strong coupling constant $\alpha_s$ measured by the DØ collaboration. The curve represents the NLO theoretical calculation for the $\Lambda_{QCD} =$ 140 MeV.

The measurement of the $\alpha_s$ by the DØ collaboration [16], for the mass value of the $W$ is,

$$\alpha_s(W) = 0.123 \pm 0.015 \; .$$

where 0.015 is the combination of the statistic and systematic errors associated with the measurement. This value for $\alpha_s$ is in agreement with other results [17] and with available calculations in LO and NLO that estimate values of $\alpha_s$ within 0.1 and 15 (Figure 2.3), at the range of energies of the Tevatron.

Theoretical comparisons in LO and NLO, also indicate that the dominating process, by one order of magnitude, for the b-quarks production in the Tevatron is the one of $\alpha_s^3$ order [13].

The description of the heavy quarks production becomes more complicated since, before or after the ocurrence of a parton-parton elementary interaction process, we can have the radiation of gluons that may produce other pairs of heavy quarks, in a cascade process that leads to a **partonic shower**.

At the other end of the $Q^2$ evolution of the strong coupling constant, when $Q \ll \Lambda$ and, thus $\alpha_s \to \infty$, processes that can no longer be described by perturbative methods, provoke the materialization of quarks into hadrons, in the form of collimated jets. These processes are called **hadronization** or **fragmentation**.

Subsequently to the appearance of these jets, a fraction of these short lived hadrons decay in a semi-leptonic form, through weak interactions, into other lighter hadrons. In such a way that, among the final states associated with the $b$-quark production in a $p\bar{p}$ collision, several leptons are found.

## 2.2 Inclusive Processes

Even if the probability of occurrence (or the $\sigma$ cross section production) of processes involving b-quarks in $p\bar{p}$ collisions, at the energy of 1.8 TeV, is reasonable ($\sigma_{b\bar{b}} = 40\ \mu b$), it is still much less than that of the occurrence of $c$-quarks, for instance, which pairs production cross section ($\sigma_{c\bar{c}}$) is in the range of 200 $\mu b$.

In this way, besides the large amount of energy of the $p\bar{p}$ beam, it is necessary that a reasonable concentration of protons and antiprotons be present so that the frequency of collisions is sufficient for the abundant production of b-quarks.

The parameter that describes this compromise is the **luminosity** ($\mathcal{L}$) of the beam[18] luminosity. In such a way that, if $\sigma$ is the total cross section production of a process, characterized by the occurrence of a certain final state, the ratio of produced events ($dN/dt$) that leads to such final state is given by:

$$\frac{dN}{dt} = \sigma\ .\ \mathcal{L} \tag{2.2}$$

The luminosity, defined as the ratio of particles (quantity of particles by unity of time) that cross an unity of area at a certain point along the beam, can be expressed in $cm^{-2}s^{-1}$. The luminosity of the $p\bar{p}$ beam in the Tevatron during the "1A run" was within the range of $1 \times 10^{30}$ through $10 \times 10^{30} cm^{-2}s^{-1}$.

If the luminosity is integrated during a certain period $T$,

$$\int_T \mathcal{L} dt$$

the amount of data collected during this period can be immediately estimated.

Cross sections are usually expressed in sub-multiples of *barn* (1 $barn = 10^{-24} cm^2$), and the integrated luminosity in inverted units ($barn^{-1}$). The luminosity integrated during the "1A run" collected by the DØ was $(13.5 \pm 0.12)\ pb^{-1}$, where 0.12 is the uncertainty due to the measurement process.

If a final state of a process presents a multiplicity of particles but not all of them are detected, *i.e.*, only one or a few of them are chosen for the characterization of it, this process is called **inclusive**.

The aim of this thesis is the determination of the inclusive $b$-quarks production cross section, through the initial determination of the final states differential production cross section that presents at least one muon, that is:

$$p\bar{p} \ \rightarrow \ bX \ \rightarrow \ \mu X$$

where $X$ represents any other non-identified particles.

The analysis of the final states with at least one muon and with the requirement of associated jets is the objective of the thesis of another member [19] of the bottom physics study group.

## 2.3 Events Simulation

The simulation of the whole process, based on the previously described partons model, since the $p\bar{p}$ inelastic collision up to occurrence of the final states with at least one muon, is fundamental in the planning of any large and complex experiment such as the DØ[20]. Through simulation is how, usually, we determine the efficiencies for several detection processes related to the distinct components of a detector.

The events generating program used in the analysis related to this thesis was the ISAJET [21] package, version 7.0. This generator is based in the Monte Carlo[4] method since, from analytic expressions related to the parameters of several sub-processes of a $p\bar{p}$ inelastic collision, it generates a pre-determined amount of events repeated in a pseudo-randomic form.

Despite the necessity of using simulation techniques, it is never enough to recall [22] Bjorken[5] comment in respect to the crescent dependence upon

[4] In a reference to the famous Monte Carlo casino.

[5] "Another change that I find disturbing is the rising tyranny of Carlo. No, I don't mean that fellow who runs CERN, but the other one, whith first name Monte. The simultaneous increase in detector complexity and in computation power has made simulation techniques an essential feature of contemporary experimentation. The Monte Carlo simulation has become the major means of visualization of not only detector performance but also of physics phenomena. So far so good. But it often happens that the physics simulations provided by the the Monte Carlo generators are carry the authority of data itself. They look like data and feel like data, and if one is not careful they are accepted as if they were data. All Monte Carlo codes come with a GIGO (garbage in, garbage out) warning label. But the GIGO warning label is just as easy for a physicist to ignore as that little message on a packet of cigarettes is for a chain smoker to ignore. I see nowadays experimental papers that claim agreement with QCD (translation: someone's simulation labeled QCD) and/or disagreement with an alternative piece of physics (translation: an unrealistic simulation), without much evidence of the inputs into those simulations."

the data acquired from simulation.

Therefore, it is important to remember that the results that can not be verified independently from the simulations, *i.e.*, results based entirely on the ISAJET package[6], depend upon the tacitly assumed models and are incorporated to the code program of the events generator.Besides this, the uncertainties associated with some parameters of the models that are constantly being adjusted, introduce systematic errors in the various results.

One of the first uncertainty sources of any method based in the partons model, is related to the partons distribution functions, mainly regarding the gluonic content of the hadrons. In the 7.0 version of the ISAJET package the distributions known as CTEQ2L are used, which were parameterized by the CTEQ collaboration[24].

One other uncertainty source is due to the way that the simulator carries out the relative corrections, that result in the partonic showers. In case of the ISAJET, these corrections are based on the Altarelli-Parisi[6, 7, 8] evolution equations.

[6]Or in any other events simulator.

• **Hadronization**

In the hadronization process, a heavy quark $Q$, with energy $E_Q$ and momentum $\vec{p}_Q$ combines itself with a light antiquark $\bar{q}$, forming a meson $Q\bar{q}$ (hadron $h$), with a fraction $z$ of energy-momentum defined by:

$$z = \frac{E^h + p^h_{//}}{E_Q + p_Q} \tag{2.3}$$

where $E^h$ is the hadron energy and $p^h_{//}$ is the momentum component of the hadron $h$ in the direction of the heavy quark $Q$.

The hadronization process cross section is given by:

$$\sigma(p\bar{p} \to hX) = \sum_q \int dz\ \sigma(p\bar{p} \to QX)\ D^h_Q(z) \tag{2.4}$$

where the distribution function $D^h_Q(z)$, that characterize the probability of occurrence of a hadron $h$ with fraction $z$ of the quark energy-momentum, is a function $f(z)$ which was normalized and parameterized by Peterson *et al.* [25, 26],

$$f(z) = \frac{1}{z[1 - 1/z - \epsilon_Q/(1-z)]^2} \tag{2.5}$$

The parameter $\epsilon_Q$ in the case of $b$ and $c$ quarks has values given by:

$$\epsilon_b = 0,006 \pm 0,003$$

$$\epsilon_c = 0,06 \pm 0,03$$

The figure 2.4 shows that for the $b$-quark, the distribution tends to be concentrated close to the value of $z = 1$. This means that, the heavy quark momentum is almost entirely transferred to the hadron, resulting in jets that remain with the direction of the heavy quark.

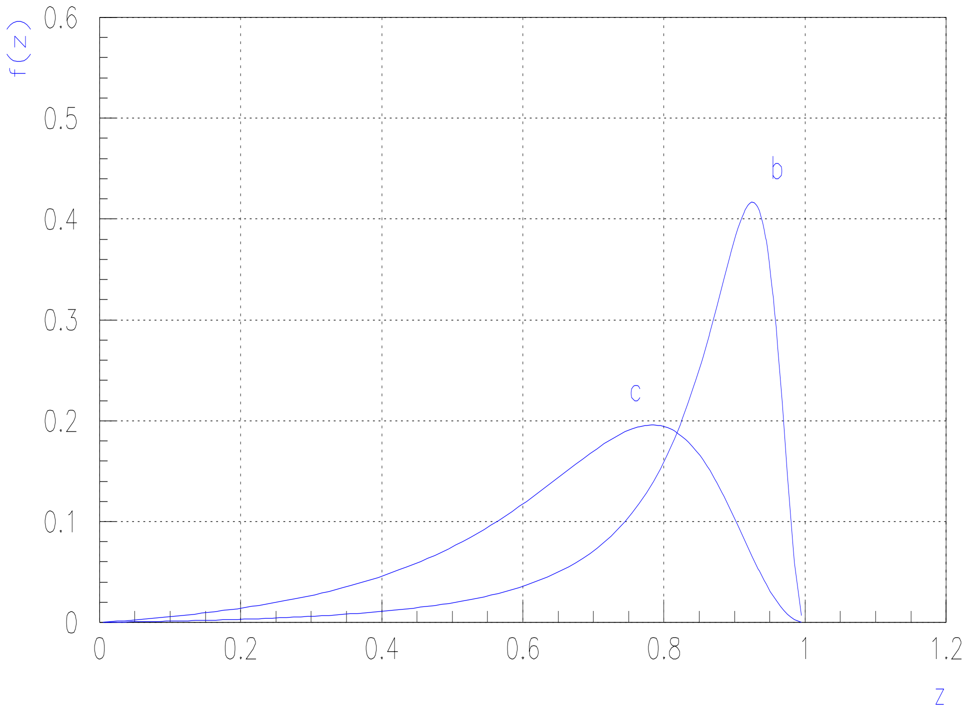


Figure 2.4: Peterson functions for $b$-quarks and $c$-quarks.

Following the Field and Feynman (FF) scheme [27, 28], which states that quark jets are independently fragmented, the ISAJET simulator generates heavy hadrons with fractions of energy-momentum originated from the Peterson function.

Finally, the semi-leptonic decays of the mesons, are simulated by an expectator model (Figure 2.5), in which the light quark $q$ does not participate in the process and the heavy quark $b$ decays in accordance with the V - A theory.

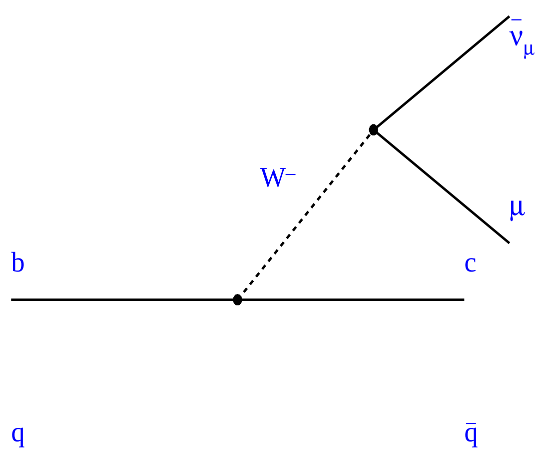


Figure 2.5: Semi-leptonic decay of a B meson ($b\bar{q}$) in the expectator model.

This decaying mechanism allows for the simulation of the spectrum shape of the resulting leptons, but the weight (normalization) of the decays of each type of mesons is fixed by the so called **branching ratios** ($Br$), which indicate the fraction of times that a particular decay occur in face of the amount of total decays of a particle. In case of mesons B[7], we use the branching ratio given by the average of the results of the experiments carried out in the LEP ([29]), with value equals to:

$$Br(B \to \mu X) = 0.11 \pm 0.005 \ .$$

## 2.4 Production of Muons

- **Semi-leptonic Decays**

The decays responsible for the muons production originated from $b$-quarks, are subjacent to the semi-leptonic decays of mesons B resulting from $b$-quarks hadronizations,

$$B \to \mu X$$

which may be direct or characterized by the presence of a D meson[8] in an intermediate state.

$$B \to DX \to \mu X \quad \text{(sequential decay)}.$$

Besides the D mesons, that appear as intermediate states of a meson B sequential decay, charming mesons can also result directly from the hadronizations and produce muons. In such case, the decay is due to the

[7]Type $q\bar{q}$ hadrons in which one of the quarks is a *bottom* or an *antibottom*.

[8]Type $q\bar{q}$ hadrons in which one of the quarks is a *charm* or an *anticharm*.

process

$$p\bar{p} \ \rightarrow \ cX \ \rightarrow \ \mu X.$$

The common characteristic pertaining to all semi-leptonic processes involving heavy quarks, is that the produced muons are accompanied by hadronic jets, *i.e.*, these muons are said to be **non-isolated**.

Two remarkable differences in the $b$-quarks and $c$-quarks decays, mainly due to the greater mass of the $b$-quark, can be utilized on the separation of the contributions of each process in the production of muons.

- The fragmentation of the $b$-quark is harder than that of the $c$-quark in the sense that the resulting B mesons carry a greater fraction of the initial quark momentum than those of the D mesons. This means that the distribution of the events originated from $b$-quarks is much closer to $z = 1$ than those originated from $c$-quarks (figure 2.4).

- The transverse component of the momentum of a muon, resulting from the decay of a $b$-quark, in relation to the initial momentum of the quark is significantly greater than that of muons originated from $c$-quark decays. This variable, called $p_T^{rel}$, introduced by the UA1 collaboration [30], constitutes the main element to establish the criteria used in this thesis for the separation of the muons resulting from $b$-quarks from those resulting from $c$-quarks.

• **Drell-Yan Processes**

One other source of muons, mainly in high $p_T$, results from the production and subsequent decay of W and Z bosons. These processes, called Drell-Yan processes, are subjacent to inclusive processes of type

$$W/Z \to \mu X \ .$$

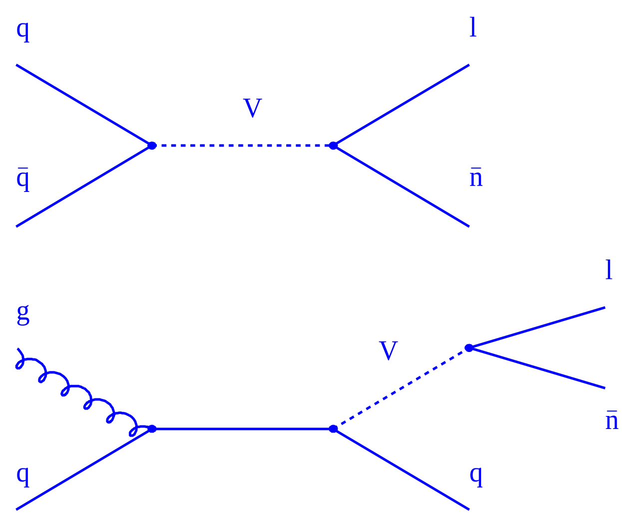


Figure 2.6: Drell-Yan type processes.

Some diagrams illustrating the Drell-Yan type processes are shown in figure 2.6, where $V \to l\bar{n}$ generically represents the processes

$$\begin{cases} W^+ \to \mu^+ \bar{\nu} \\ W^- \to \mu^- \bar{\nu} \\ Z \to \mu^+ \mu^- \end{cases}$$

Although these processes contribute at a very low extent to the muon production total cross section, as the associated branching ratios are very low,

$$\begin{cases} Br(W \to \mu\nu) \times \sigma(p\bar{p} \to W) \sim 600 \ pb \\ Br(Z \to \mu\mu) \times \sigma(p\bar{p} \to Z) \sim 58 \ pb \end{cases}$$

they can become a very significant background in the region of high $p_T$, since the cross section of muons resulting from $b$ is also small in this region. Besides this, differently from the semi-leptonic decays of the mesons, the characteristic of the muons originated from the Drell-Yan type processes is that they are isolated, *i.e.*, they are not associated with jets. Accordingly, muons associated with a great unbalance of energy or pairs of muons associated with a great invariable mass, are generated.

• **Pions and kaons decays**

One other abundant source of muons, mainly with low transverse momentum, results from the decays of pions ($\pi$), the particles produced in the largest amount in a $p\bar{p}$ collision, and to a smaller extent from the decays of kaons ($K$), before being absorbed by the detector itself.

This inclusive muons production process, generically represented by:

$$\pi/K \to \mu X$$

was simulated by another member [31] of the bottom physics study group of the DØ collaboration, from the estimation of the muons production differential cross section, $(d\sigma/dp_T)_\mu$, resulting from $\pi/K$ mesons. This cross section was determined by the convolution of the $\pi/K$ mesons production differential cross section, $(d\sigma/dp_T)_h$ , with the probability $\mathcal{F}(p_T^\mu, p_T^h)$ that a hadron $h$ (pion or kaon) with transverse momentum $p_T^h$ decay into a muon with transverse momentum $p_T^\mu$.

$$\left(\frac{d\sigma}{dp_T}\right)_\mu = \int dp_T^h \; \mathcal{F}(p_T^\mu, p_T^h) \; \left(\frac{d\sigma}{dp_T}\right)_h \tag{2.6}$$

The hadrons production cross section was obtained from the inclusive production cross section of charged hadrons up to 10 GeV measured by the CDF collaboration at 1.8 TeV in the Fermilab. The decays probabilities, from the data taken at 630 GeV by the UA2[32] and UA5[33] collaborations at the CERN and, subsequently, taking into consideration the characteristics of the DØ detector. Other charged particles were not considered and such estimation was taken for the central region of the detector and for $3.5 < p_T < 12$ GeV, where muons of pions decays dominate the ones of kaons decays by a factor 4.

These are the main sources of muons associated with the $p\bar{p}$ collisions. Another unavoidable background source are the cosmic rays.

• **Cosmic Rays**

Any particles flow that reach the earth atmosphere with energy greater than 100 MeV is generically called cosmic rays. Of unknown origin, they are primarily constituted to a large extent by protons (around 90%), nucleons of helium (around 7%) and a very small parcel of electron-positron pairs (around 1%) and photons (around 0.01%), that literally arrive from all directions.

As soon as they penetrate the atmosphere, they interact with the medium and, through a cascade process, generate more and more secondary particles constituting the so called shower. As the majority of the incident particles are protons, in the interaction of these ones with the nucleons of the medium, the generated particles are, in the majority, pions.

This process is completed with the decays of pions into muons and neutrinos, which constitute the so called hard component of the cosmic rays, that reach the earth surface.

## 2.5 Rapidity

At the circular collider tunnel of the Tevatron, the DØ detector is located around one of the intersection points of the protons and antiprotons beams. In the vicinity of this colliding point, called the **primary vertex**, the $p\bar{p}$ beam defines a convenient direction to be taken as the polar coordinates axis (figure 2.7).

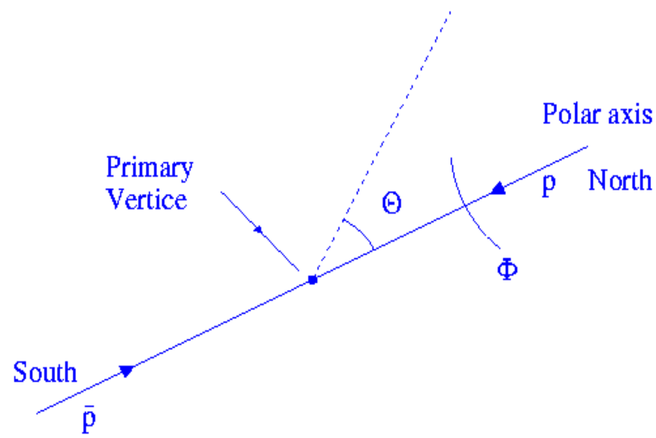


Figure 2.7: Polar ($\theta$) and azimuthal ($\phi$) coordinates in the DØ detector.

In the figure 2.7, the polar angle $\theta$ is defined from the protons beam in such a way that $\theta = 0$ corresponds to the region between the primary vertex and the geographical north (from where the protons arrive). The azimuthal angle $\phi$ is measured around the $p\bar{p}$ beam from a plane parallel to the ground, in the west-east right-hand direction, in such a way that $\phi = \pi/2$

corresponds to the top of the detector. Generally, only the components of quantities transversal to the beam are invariant under a **boost**[9] of Lorentz at the direction of the beam. However, the expression (2.7) of the **rapidity** ($y$) of a particle with energy $E$,

$$y = \frac{1}{2}\, log\, \left(\frac{E + p_L}{E - p_L}\right)\ . \tag{2.7}$$

where $p_L$ is the component of its momentum along the beam (longitudinal component), shows that the rapidity of any particle resulting from the Tevatron collisions is invariant[10] under a boost of Lorentz at the $p\bar{p}$ beam direction. As a consequence of this invariance, the distribution of events, such as the accounting of the occurrence of a certain type of particle, according to $p_T$ or $y$ ranges, have invariant forms under any boost of Lorentz at the $p\bar{p}$ beam direction.

The rapidity, at the high energies limit, when the energy of a particle is much greater than its mass ($E \gg m$), tends to a purely geometrical quantity called **pseudo-rapidity** ($\eta$), that depends solely on the polar angle (equation 2.8).

$$\eta = -log\, \left|tan\, \frac{\theta}{2}\right| \tag{2.8}$$

The pseudo-rapidity is measured from a perpendicular to the $p\bar{p}$ beam, at the direction contrary to the $\theta$ angle, and allows for a convenient sub-division

[9]Transformation of Lorentz along a spatial direction between references with origins (of time and space) initially coincident.

[10]See appendix B.

of the detector itself.

The DØ detector and its sub-systems are, basically, divided into two regions of $\eta$ (figure 2.8) ranges:

- **central** : $|\eta| < 1$
- **frontal** : $|\eta| > 1$

By this way, parameters associated with certain spatial regions, like detection efficiencies are also parameterized in terms of $\eta$ ranges.

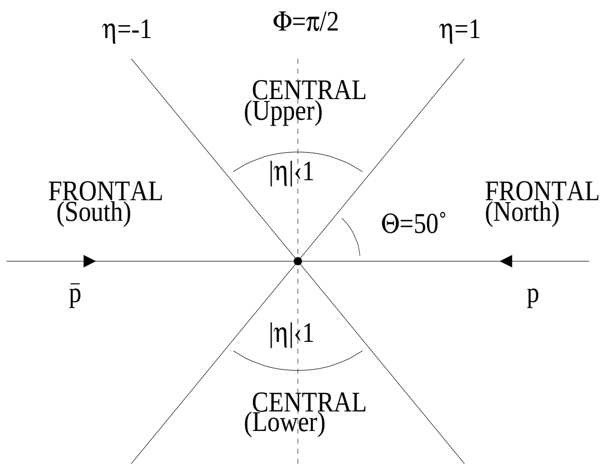


Figure 2.8: Typical regions of the detector in terms of pseudo-rapidity, $\eta$, of polar angle, $\theta$, and of the azimuthal angle, $\phi$.

## 2.6 Cross Sections

Once the contributions of the main processes capable of producing muons are estimated, the $b$-quarks production cross section is determined in three steps [4].

• The first one consists in the calculation of the inclusive muons production differential cross section over the rapidity range ($\Delta y$), according to the expression:

$$\frac{1}{\Delta y}\left(\frac{d\sigma}{dp_T}\right)_{\mu} = \frac{1}{\Delta y}\ \ \frac{N^{\mu}}{\int \mathcal{L}\ dt\ .\ \varepsilon} \tag{2.9}$$

where $N^{\mu}$ is the observed quantity of muons that are not originated from cosmic rays, by unity of momentum in GeV, *i.e.*,

$$N^{\mu} = N^{\mu}_{total} - N^{\mu}_{cósmicos}\ .$$

$\int \mathcal{L}dt$ is the integrated luminosity of the $p\bar{p}$ inelastic collisions related to the collected data and $\varepsilon$ is the global efficiency of muons detection.

• In the second step, after the subtraction of the muons originated from cosmic rays, those resulting from $W/Z$ bosons decays ($N^{\mu}_{W/Z}$) are also subtracted and multiplied by the fraction ($f_b$) of those resulting from $b$-quark decays,

$$\left(N^{\mu}_{total} - N^{\mu}_{cósmicos} - N^{\mu}_{W/Z}\right)\ .\ f_b$$

.

The inclusive muons production differential cross section originated from $b$-quarks over the rapidity range is then calculated by:

$$\frac{1}{\Delta y}\left(\frac{d\sigma}{dp_T}\right)_{b\to\mu} = \frac{1}{\Delta y}\ \frac{\left(N^{\mu} - N^{\mu}_{W/Z}\right) . f_b . f_p}{\int \mathcal{L}\ dt\ .\ \varepsilon} \qquad (2.10)$$

where $f_p$ is a correction factor function of $p_T^{\mu}$ due to the muons momentum resolution.

The results of this thesis, related to the muons cross sections, refer to the data acquisition in the central region of the DØ detector, defined by

$$|\eta| < 0.8$$

The analysis of the data related to the central region of the detector, defined by

$$2.2 < |\eta| < 3.3$$

is the objective of the thesis of another member [34] of the bottom physics study group of the LAFEX.

• In the third and last step, the $b$-quarks inclusive production cross section is derived, following a method established by the UA1 collaboration [30] of the CERN and also utilized by the CDF collaboration [35] at the Fermilab.

Accordingly, the inclusive $b$-quark production cross section integrated after a certain $p_T^{min}$ is given by:

$$\sigma^b(p_T^b > p_T^{min}) = \frac{1}{2}\ \sigma_b^{\mu}(p_T^{\mu 1} < p_T^{\mu} < p_T^{\mu 2})\ \left(\frac{\sigma^b}{\sigma^{\mu}}\right)_{ISAJET} \qquad (2.11)$$

where $\sigma_b^\mu(p_T^{\mu 1} < p_T^\mu < p_T^{\mu 2})$ is the inclusive muons differential production cross section originated from $b$-quarks over the rapidity range, integrated in the range $p_T^{\mu 1} < p_T^\mu < p_T^{\mu 2}$. The factor 1/2 represents the average of the $b$ and $\bar{b}$ production cross sections from measurements of $\mu^+$ e $\mu^-$.

For each $p_T^\mu$, $p_T^{min}$ is determined, by the $b$-quarks and muons production cross sections derived from the ISAJET generator, in a way that 90% of the muons in the range originated from $b$-quarks with $p_T^b > p_T^{min}$, e $(\sigma^b/\sigma^\mu)_{ISAJET}$ is the ratio between the cross sections utilized for the determination of the $p_T^{min}$.

In order to conclude the program of study of this thesis and of the other physics study groups of the DØ collaboration, a detector with certain characteristics was necessary. The DØ detector, that will be described in the next chapter, although being a detector that fulfills a wide range of objectives, completely satisfies the main requirements of its study groups.

# Chapter 3

# The DØ Detector

The DØ collaboration has five large organized groups for the study of physics, each of them with their specific objectives:

- **Top**
- **Bottom**
- **QCD**
- **W/Z**
- **New phenomena**

Generally speaking, all of them are related to the heavy quarks production or even to the possibility of identification of new particles in $p\bar{p}$ collisions. And, for the achievement of their objectives, they required a detector with the following characteristics:

- excellent identification of leptons

- optimum measurement of hadronic jets
- determination of the occurrence of neutrinos

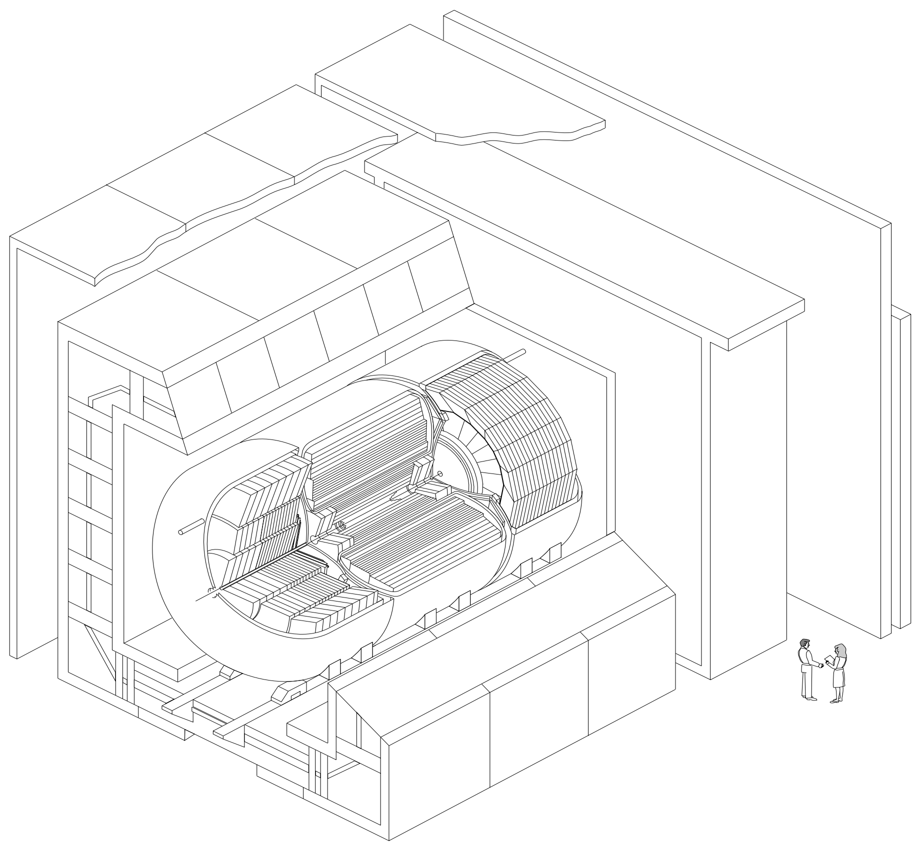

Figure 3.1: The DØ Detector.

necessary for the reconstruction of a hadronic collision in channels which final states result from semi-leptonic decays. A complete description of the DØ detector is found in the reference [3]. The following description emphasizes only the parts in which the LAFEX group has contributed in a decisive way, both in the *hardware* and *software* areas. The parts of the detector that received more contributions from the LAFEX group, were chosen based on the main physics results extracted by the group.

The DØ detector [36] was designed and constructed to fulfill these requirements. Its main sub-systems, the **Central Detector**, the **Calorimeter** and the **Muons System**, reflect this choice (figure 3.1).

## 3.1 Central Detector

The nearest sub-system to the beam line, the **central detector** (**CD**) of the DØ (figure 3.2), is the system that identifies the trajectories (tracks) of charged particles generated in the $p\bar{p}$ collision, whenever they get away from the interaction point. This information can be used by the calorimeter to decide whether an electromagnetic shower (section 3.2) was caused by electrons, photons ($\gamma$) or neutral pions ($\pi^0$).

Besides the reconstruction of tracks, the central detector also allows for the vertex determination (origin points) of the several decays and is also referred to as the **tracking system**.

The central detector **CD** is composed by four sub-detectors (figure 3.2):

- The **Vertex Detector** (VTX).
- The **Transition Radiation Detector** (TRD).

- The **Central Drift Chambers** (CDC).

- The **Frontal Drift Chambers** (FDC).

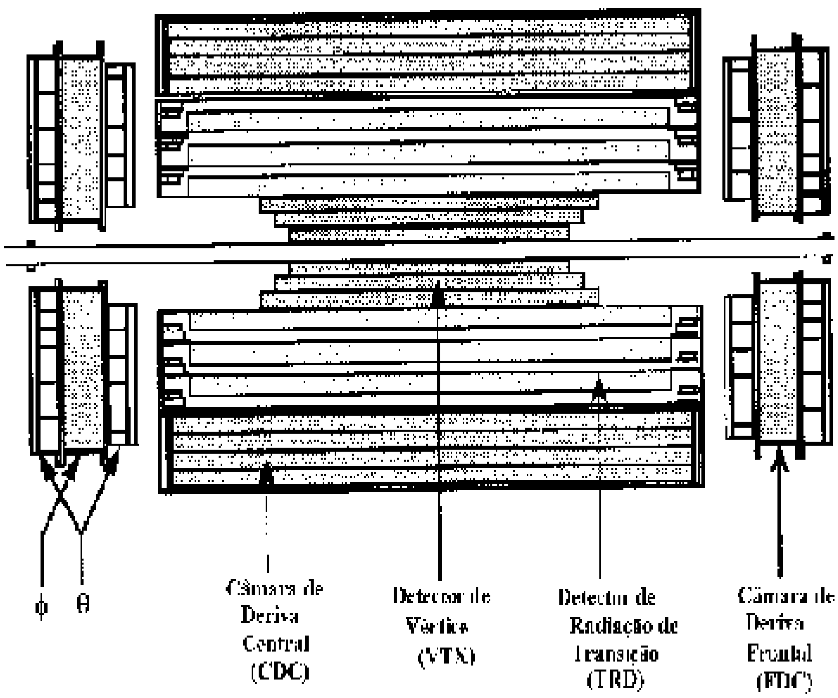


Figure 3.2: Side-view of the DØ Central Detector (CD).

The drift chambers (CDC and FDC) and the vertex detector (VTX) are ionization chambers in which a charged particle that moves through a gas, ionizes it around its trajectory.

By means of an adequate arrangement of wires submitted to potentials in the range of some kilovolts and through the establishment of an electrostatic field in the interior of the chambers, charge pulses due to the drift of ions and electrons are collected and, from the time of the arrival of the charges at the wires, information related to the location of the ionizing particle is obtained.

The performance tests [3] of the VTX and of the CDC were carried out with $p\bar{p}$ beams, and with cosmic rays in the case of CDC. For the VTX the typical spatial resolution was in the range of 50 $\mu m$ and the efficiency for the distinction of two separate tracks of at least 0.6 $mm$ was approximately 90% or more. In the case of the CDC, the spatial resolution varies from 100 $\mu m$ a 200 $\mu m$ for drift distances of 1 $cm$ e 5 $cm$, respectively. The efficiency of the CDC for the resolution of two tracks is 50% for separations of 1.7 $mm$ and, 90% for separations of 2.5 $mm$. The table 3.1 summarizes these characteristics.

| | Spatial Resolution | Efficiency (2 tracking resolution) |
|---|---|---|
| VTX | $\sim 50$ $\mu m$ | 90%, for separation $> 0.6$ $\mu m$ |
| CDC | $< 230$ $\mu m$ | 90% for separation $> 2.5$ $mm$ |

Table 3.1: Resolutions and efficiencies of the VTX and CDC of the DØ.

The TRD, located between the VTX and the CDC, is constituted by three layers of radiators separated by ionization chambers. The radiators are constituted by polypropylene foils immersed in nitrogen. When charged particles, highly energized, pass through the radiator, crossing the interfaces of the polypropylene foils and the nitrogen, the so called transition radiation occurs, at the X-ray band, proportionally to the charged particle momentum. This characteristic is utilized for the distinction between electrons and pions, since the electrons resulting from $p\bar{p}$ collisions are much more energetic than the pions.

Correlating the collected ionized charge and the energy deposited in the calorimeter it is even possible, in principle, to distinguish between electrons and muons.

Located at the extremities of the other sub-systems of the central detector (CD), and perpendicular to the beam, the frontal drift chambers (FDC) extend the tracking capacity of charged particles, up to distances of $\sim 5\ cm$ from the beam lines, which corresponds to a geometrical coverage of $1.4 < |\eta| < 3.1$.

Once the DØ detector does not have a central solenoid, which could submit the particles to a magnetic field, the tracks are straight lines and, thus, neither the momentum nor the charges sign of the particles can be measured by the central detector.

## 3.2 The Calorimeter

Around the central detector, it is located the **calorimeter** which, essentially, is the device that measures the energies of neutral or charged particles, absorbing them. In the absence of a central magnetic field, the

DØ calorimeter, besides measuring the energy of electrons, photons and jets, in conjunction with other sub-detectors, has an important role in the identification of the particles and in the energetic balance, that makes it possible to verify the presence or not of neutrinos.

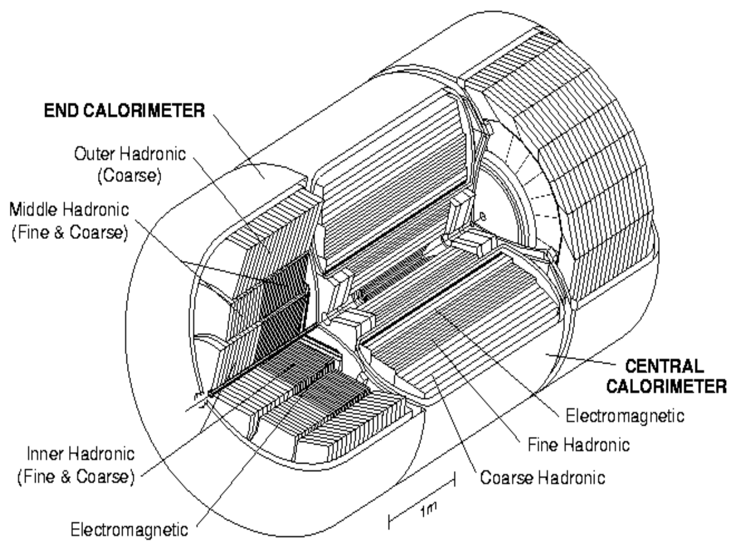


Figure 3.3: The DØ Calorimeter.

Since the first decisions of the DØ collaboration, the argon was chosen as the active medium for the calorimeter, *i.e.*, the medium to be ionized by electromagnetic showers or hadrons. This choice has implicated in certain characteristics, such as unit gain, simple calibration and flexibility for segmentation, which compensate the cryogenic apparatus involved, and resulted in a compact calorimeter (figure 3.3) composed of three parts in accordance with the kinematical regions involved in the collision process:

- the **central calorimeter**, that covers the region of $|\eta| < 1,2$.
- and one pair of **frontal calorimeters**, that cover the regions within $1.1 < |\eta| < 4.5$.

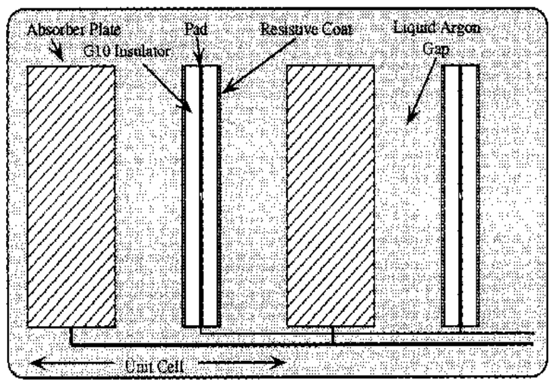


Figure 3.4: Basic cell of the DØ calorimeter.

Cosmic rays, when penetrating the atmosphere, interact with the medium generating more and more particles (*showers*), in a cascade process. In the case of the DØ calorimeter, a shower is generated when the particles resulting from $p\bar{p}$ collisions pass through absorbing medium (steel, plumb, uranium) and then ionize layers of liquid argon that functions as a detector.

The figure 3.4 shows schematically the cells of uranium absorbers immersed in liquid argon and a signals read out system. These cells are radially aligned, constituting the so called **read out towers** and segmented according to intervals of $\Delta\eta = 0.1$ e $\Delta\phi = 0.1$.

Generally, the showers that occur in a calorimeter can be divided into electromagnetic and hadronic, what causes a corresponding sub-division of the calorimeter into electromagnetic and hadronic sections.

• **Electromagnetic Showers**

When an electron ($e^-$) or a positron ($e^+$) at high energies ($> 10\ MeV$) penetrates a medium, interacting with the coulombic field generated by the neutrons, they are disaccelerated producing photons (*bremsstrahlung* – braking radiation).

On the other hand, photons at high energies, in the presence of nucleons, can materialize and produce electron-positron pairs. Accordingly, when electrons, positrons and photons pass through a dense medium, they generate secondary electrons, positrons and photons in a cascade process that constitutes the so called electromagnetic shower.

This cascade keeps going on until the resulting particles, with sufficiently low energies, do not irradiate nor form $e^+e^-$ pairs anymore and the dominating loss process starts to be by ionization of the medium.

• **Hadronic Showers**

In the case of hadrons, the showers are mainly caused by the energy loss due to inelastic collisions with the nucleons, that produce secondary hadrons and so on. By analogy, the process continues until the loss by ionization becomes dominating.

One important characteristic of these processes is that the fractional energy loss by the distance travelled by the particle along its trajectory,

$$\frac{1}{E}\frac{dE}{dx}$$

is a constant that is a function of the material, called **radiation length** ($X_0$), in the electromagnetic case, and **nuclear interaction length** ($\lambda$), in the hadronic case.

The table 3.2 shows the constants of the DØ central calorimeter which main absorbing medium is the uranium, that estimate the energy loss and the thickness of the hadronic and electromagnetic parts in terms of these constants.

| Uranium | Central Calorimeter | |
|---|---|---|
| | Electromagnetic | Hadronic |
| $X_0 = 3.2$ mm | 20.5 $X_0$ | 32.9 $X_0$ |
| $\lambda = 10.5$ cm | 0.76 $\lambda$ | 3.2 $\lambda$ |

Table 3.2: Constants and thickness of the DØ central calorimeter.

Hadronic showers have a stronger penetrating power and, therefore, the calorimeter sections for the measurement of hadrons energies are external to the electromagnetic sections.

In principle, there is no reason for the calorimeter response, indicated by the relation between the measured signal and the energy of the incidental particle, to be the same for both hadronic and electromagnetic showers. In fact, the response tends to be lower for hadronic showers, once neutrinos and muons, produced from pions and kaons[1] decays, escape from the calorimeter.This response is well expressed by the $e/\pi$ relation, *i.e.*, by the relation between the calorimeter response for electrons and pions.

The tendency of the $e/\pi$ relation to be smaller than 1 can be compensated by components, that generate electromagnetic showers, contained in a hadronic shower like the photons ($\gamma$) derived from decays of $\pi^o$ e J/$\psi$.

If the $e/\pi$ relation is close to 1, the fluctuation of the energies deposited by the hadrons in the calorimeter through different showers, do not affect the resolution in the energy measurement of the calorimeter[2]. In the case of the DØ calorimeter, the $e/\pi$ relation is in the range of 1.11 at an energy of 10 GeV and drops to 1.04 at an energy of 150 GeV.Even if the $e/\pi$ relation is very close to 1, the fluctuation on the quantity of electrons released from ionization provokes fluctuations in the energy deposited in the calorimeters, degrading the resolution in the energy measurement of the calorimeter.

Some other sources of energy fluctuation in the DØ calorimeter are:

- hadrons that escape (*hadron punchthrough*) from the calorimeter.
- noise in the active layers (radioactivity) of the uranium.

[1]These decays are a source of signals that constitute a background in the heavy quarks production.

[2]In this case, the calorimeter is said to be *compensated*.

- electronic noises.

- fluctuations in the high-tension.

All these uncertainties resulted into a parameterization of the energy measurement resolution of the DØ calorimeter, such as

$$\left(\frac{\Delta E}{E}\right)^2 = C^2 + \frac{S^2}{E} + \frac{N^2}{E^2}$$

where C is a constant that represents uncertainties in the calibration, S represents fluctuations in the form of the showers and N is due to the noises (Table 3.3).

| | C | S | N |
|---|---|---|---|
| Electrons | $0.003 \pm 0.002$ | $0.157 \pm 0.005\ (GeV)^{1/2}$ | $\sim\ 0.140\ GeV$ |
| Pions | $0.032 \pm 0.004$ | $0.41 \pm 0.04\ (GeV)^{1/2}$ | $\sim\ 1.28\ GeV$ |

Table 3.3: Resolution parameters of the DØ calorimeter.

## 3.3 Muons System

This part of the detector is the one where the contribution from the LAFEX group was important and decisive for the quality of the collected data.

Although muons decay into electrons during an average time of 2.2 $\mu s$, the travel time of a muon in any direction inside the DØ detector is in the range of nanoseconds. Since they don't interact strongly and as they have a very large mass ($\approx 200\ m_e$) to start an electromagnetic shower, practically they may be considered as stable particles inside the detector.

The DØ muons system [37] is constituted of three layers of ionization chambers (**A**, **B** & **C**) and of magnetized iron toroids, with currents of 2500A that generate a magnetic field in the range of 2T, between the **A** & **B** (figure 3.5).

The muons system consists of two sub-systems:

- **WAMUS** – that has a central toroid (**CF**) that covers a region of $|\eta| < 1$ and two toroids transversal to the beam (**EF**) that cover the regions of $1 < |\eta| < 2.5$.
- **SAMUS** – that has two small toroids that cover the region of $2.5 < |\eta| < 3.6$.

Due to the necessity to support the calorimeter some regions, the lower part of the detector is not entirely covered by the muons chambers and for

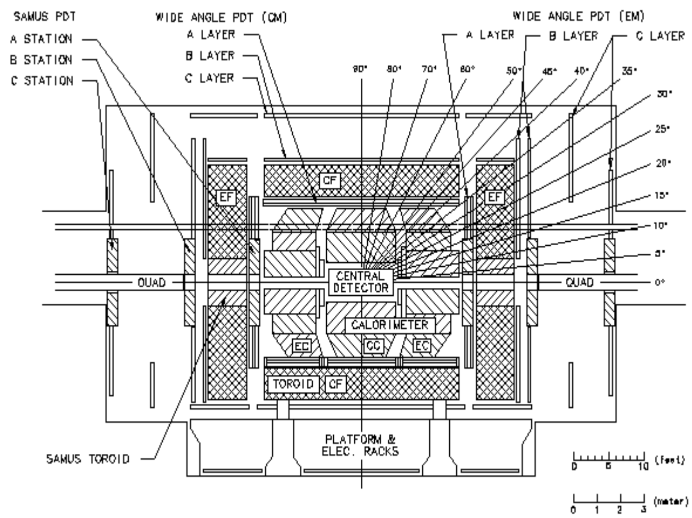


Figure 3.5: Side-view of the DØ detector.

this reason was removed from the analysis.

The greater the quantity of material between the muons system and the collision point is, the smaller will be the background due to the hadrons that escape from the calorimeter (*hadron punchthrough*). The figure 3.6 shows how the thickness of the detector, in units of nuclear interaction length ($\lambda$), varies with the polar angle ($\theta$). At $\eta = 0$, the minimum momentum measured for a muon to cross the calorimeter and the toroids is in the range of 3.5 GeV. For regions nearer to the beam (SAMUS) this momentum is in the range of 5 GeV.

The reconstructed trajectory of a muon through the system has two inclinations. One is determined by the chambers of the **A** layer, through

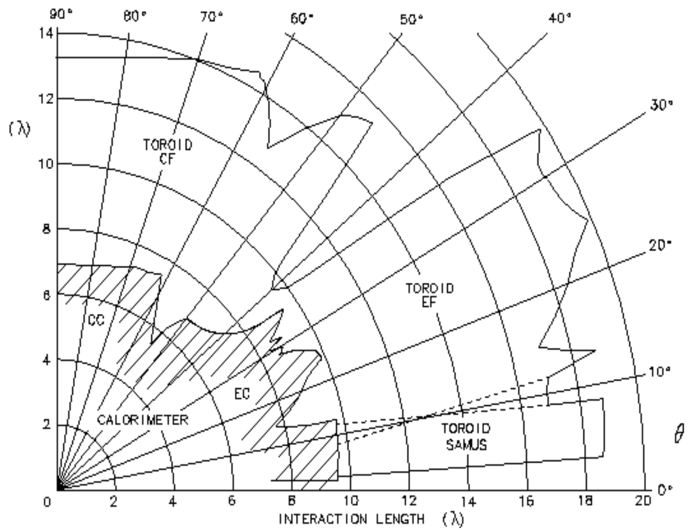


Figure 3.6: Thickness of the DØ detector in units of nuclear interaction length ($\lambda$) as a function of the polar angle ($\theta$).

an adjustment to the tracks determined by the central detector (CD) and through a minimum amount of energy deposited by the muon in the calorimeter (besides utilizing the primary vertex indicated by the central detector). The other inclination is determined by the chambers of the **B** & **C** layers. By this way, also utilizing the value of the magnetic fields in the toroids, the muon momentum is calculated.

• **WAMUS**

This sub-system is divided into 164 chambers arranged in three cubic forms, constituting the **A**, **B** & **C** layers, and completely involves the other detection sub-systems of the DØ, the Calorimeter and the Central Detector.

The basic element of the WAMUS, the so called **PDT** (*Proportional Drift*

*Tube*) [38, 39], consists of a large ionization tube in which the time difference in the collection of the data, at both extremities of a wire in its interior, allows for the determination of the gas ionization by a muon along the tube, with a resolution in the range of 10 through 20 cm.

Besides this, the tube casing is divided in two groups of plates (**PAD**) that constitute a big capacitor, at such a geometry that, through the measurement of the stored charge, a finer resolution of the gas ionization position is achieved ($\approx 2$ mm) [40].

The **B** & **C** layers are constituted of 3 planes of PDT and the **A** layer by 4 planes.

The number of **PDT** in each plane varies from 14 through 24 and the length from 2 through 6 m, in such a way that the total number of PDT is 11386.

Whenever a muon crosses a tube (PDT) this generates a single *bit* of output information, that constitutes the input for the muons trigger system (section 3.4).

◦ **Momentum Resolution**

The position and the momentum of a muon are determined by information provided by the muons chambers, through the central detector chambers and through the magnetic field in the toroids.

The calculation algorithm of the momentum utilizes a method based on minimum squares considering 7 parameters: 4 parameters that describe the position of a muon track before the calorimeter, 2 parameters that describe the muon deflection due to multiple scattering and one parameter associated with the deviation of the muon through the magnetic field established in the toroids.

The resolution in the measurement of the momentum was estimated from the generation of a muon track sample subject to the degrading of the chambers. The function that adjusted better to the data is well expressed in terms of the inverse of the momentum $X = 1/p$, and was parameterized as:

$$\left(\frac{\Delta X}{X}\right)^2 = [0.18\,(1-2X)]^2 + \left(\frac{0.008}{X}\right)^2$$

where the first parcel is the contribution due to the multiple coulombic scattering, and the second parcel is due to the magnetic field of the toroid.

• **SAMUS**

Due to the high level of occupation in the central region, the SAMUS sub-system utilizes smaller tubes (PDT). It is also constituted of three layers (stations) each consisting of three planes of PDT.

Contrarily to the WAMUS, where the tubes in each layer are parallel, the PDT planes are constituted of non-parallel tubes to solve ambiguities in the location of the muons ionization.

## 3.4 Trigger and Data Acquisition

With a typical collision rate of 290 kHz at the $p\bar{p}$ beam intersection regions of the Tevatron and a luminosity of $5 \times 10^{30} cm^{-2} s^{-1}$ in the DØ around 3/4 of the collisions are inelastic.

Due to the impossibility to collect and process data from each collision, it is necessary to have some device for the selection of *interesting* events for storage and subsequent analysis. This *on–line* selection process constitutes a trigger system.

A diagram of the DØ trigger system is shown in figure 3.7. This diagram will be clarified along with the description of its parts. The description will not necessarily follow the hierarchy of figure 3.7.

Basically, this system is divided into three hierarchic levels:

- **Level 0 General Trigger**
- **Level 1 General Trigger**
- **Level 2 General Trigger**

### 3.4.1 Level 1 General Trigger

The choice of starting the description with the Level 1 General *Trigger* is due to the fact that this is the heart of the system, responsible for the combination of the individual results from the various components of the

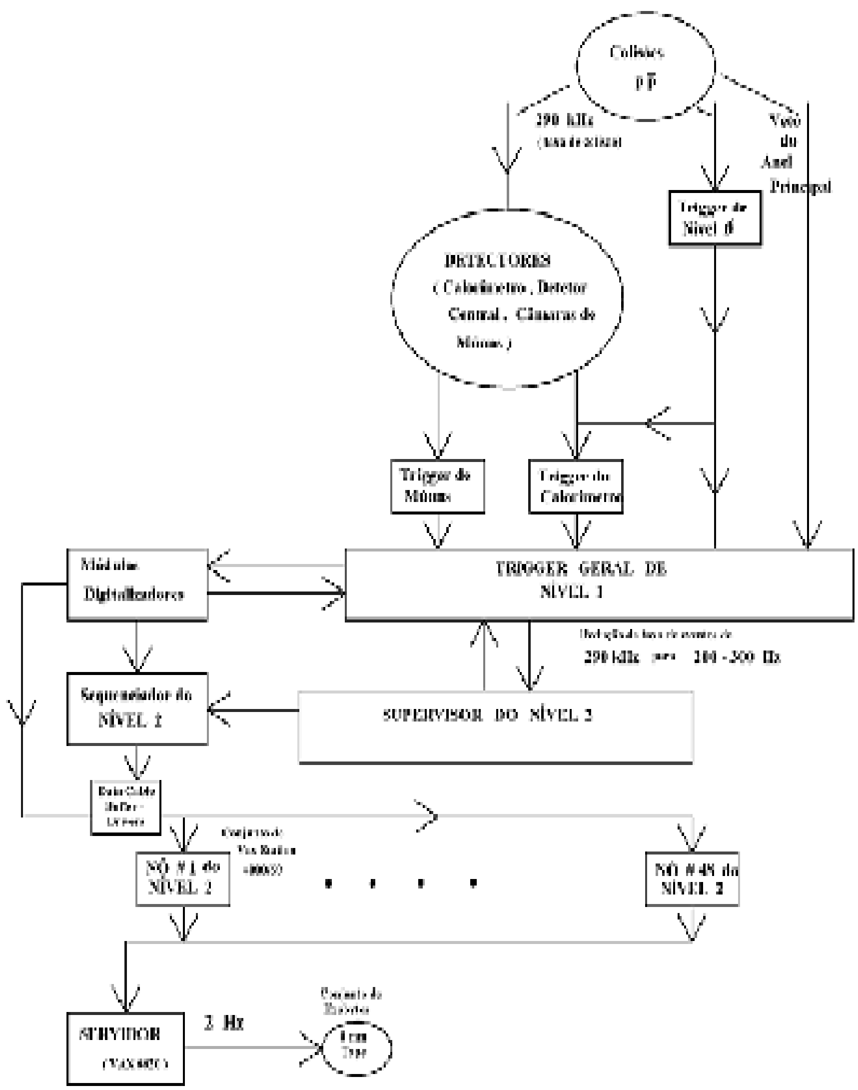


Figure 3.7: DØ *Trigger* System.

detector into a group of global decisions, commanding the read out of the digitalization modules and intermediating them with the Level 2.

The **Level 1** is a collection of electronic circuits that receive the signals from the various sub-detectors. Without considering the **dead time** [3], its decision can occur within an interval between two collisions which lies in the range of 3.5 $\mu s$.

Whenever the output rates from Level 1 are still high, it is necessary to introduce one more hierarchy in the system, called **Level 1.5 General Trigger**, which has a longer decision time and introduces a dead time in the system.

The central aim of the Level 1 is to reduce the 290 kHz events rate to a rate within 200 through 300 Hz. An event accepted by the Level 1 is entirely digitized and transferred to one of the 48 nodes of the Level 2. These, are general use computers, dedicated, that process the events in parallel. They make a quick reconstruction of the event and may utilize filtering programs that decide whether the event must be kept or disregarded, *i.e.*, with a power of veto. If the event passes through Level 2, it is transferred to a tape magnetic recording system.

Its primarily entry consists of 256 **logical terms**, where each term is a *bit* that indicates whether any condition is satisfied by the present event. These terms are reduced to a group of 32 **specific trigger bits**.

[3] Period in which the system is not able to receive information, *i.e.*, it does not record the occurrence of any event.

Each *trigger bit* can be programmed to accept or reject certain groups of logical terms and, besides this, can be programmed to reduce the decision rate by a whole factor $N$ (*prescaling*).

The digitalization circuits are located in 86 standard modules (VME), in a mobile platform (MCH), within 10 m away from the collision tunnel. For the read out purpose, these modules are grouped into 32 **geographical sectors** that correspond to each **specific trigger bit**.

If a level 1.5 decision is necessary, the cycle is delayed, but more elaborated criteria may select the events.

The main entry channels in the Level 1 are: **Level 0**, **Main ring vetoes**, **Calorimeter trigger** and the **Muon system trigger**.

• **Level 0**

The so called Level 0 is designed to detect inelastic collisions and perform a quick reconstruction and determination of the primary vertex position.

It consists of two groups of detectors, located at the end of the central detector frontal part. These detectors are plastic scintillators attached to photo–multiplier tubes.

Its efficiency is 99% for inelastic collisions and, from the comparison of the arrival time of two signals from two detectors an estimation ($z_{fast}$) with resolution of $\pm 15$ $cm$ is possible in a period of 800 $ns$ after the collision. A more accurate determination ($z_{slow}$) with resolution of $\pm 3.5$ $cm$ is carried out in a period of 2.1 $\mu s$.

• **Main ring vetoes**

During the normal operation of the Tevatron, the main ring is utilized for the production of anti-protons, at a 2.4 $\mu s$.

Once the beam crosses the detector, losses, mainly, at the instant of the beam injection, lead to an inhibition (veto) of the system for 0.4 $s$, until the high-tension that feeds the sub-detectors stabilizes.

Even during the normal passing of the protons and antiprotons packages, losses can happen and are eliminated by the veto in the logical term called microblanck, which is the time that the package takes to pass through the muons system ($\pm 800$ $ns$).

• **Calorimeter trigger**

It is a quick decision *trigger* (of level 1), within the interval of 2.4 $\mu s$, that receives signals from the calorimeter cells, digitizes it and calculates a certain number of sums:

- Total electromagnetic energy: $\sum_i E_i^{em}$

- Total hadronic energy: $\sum_i E_i^{had}$

- Total transverse electromagnetic energy: $E_T^{em} = \sum_i E_i^{em} sen\theta_i$

- Total transverse hadronic energy: $E_T^{had} = \sum_i E_i^{had} sen\theta_i$

- Total transverse energy: $E_T = E_T^{em} + E_T^{had}$

- Missing transverse energy: $\not{E}_T = \sqrt{E_x^2 + E_y^2}$

where
$$\begin{cases} E_x = \sum_i (E_i^{em} + E_i^{had}) sen\theta_i cos\phi_i \\ E_y = \sum_i (E_i^{em} + E_i^{had}) sen\theta_i sen\phi_i \end{cases}$$

These quantities are compared with a group of pre–established limits and, from these comparisons, *trigger terms* that are the entry signals for the Level 1 general trigger result.

These procedures allow for the subsequent specification of selection criteria, such as:

- Total transverse energy above 140 GeV ($E_T > 140$ GeV).
- Missing transverse energy above 20 GeV ($\not{E}_T > 20$ GeV).
- One electromagnetic tower above 5 GeV at central region.

• **Muons trigger** The entry signals for the muons trigger system are the so called *trigger latches*, *i.e.*, the group of 16000 bits associated to each one of the muons system PDT, that represents each muon that passes through it or a **hit**.The Level 1 divides the muons system into five regions:

- central (CF)
- frontal–north (EFN)
- frontal–south (EFS)
- SAMUS–north (SN)
- SAMUS–south (SS)

In each region the trigger searches for patterns of *hits* consistent with a muon originating from the nominal interaction point.

In the majority of the regions hits in at least 3 planes of a chamber are required, except at the central region where in some sectors hits in only 2 planes are required.

The trigger counts the number of track candidates in each region and compares them with a group of pre–determined tracks. Any appropriate trigger term is sent to the Level 1 general trigger.

The muons trigger is not capable to distinguish between muons of different momenta since the tracks accepted by it are very scattered.

There is also a level 1.5 muons trigger capable of imposing a transverse momentum criteria, requiring a closer match between the muon tracks. However, due to the combinatorial noise from different parts of the electronics, specially at the region near to the beam line (SAMUS), this process brings a dead time to the system.

In a more detailed way, the *trigger latches* are conducted from the detector to a mobile platform (MCH), up to the type VME modules, where the address cards (MAC), which have a univocal relation with the chambers of the WAMUS, combine close hits into centroids that satisfy the pre-established coincidences.

Two types of centroids are determined. One associated with a granularity of half a cell (5 cm for the WAMUS) and constitutes the basic unit of the level 1.5 muons trigger. The other one with a greater granularity (15 cm for the WAMUS) constitutes the basic unit for the level 1 muons trigger.

The centroids with smaller granularity are sent to the electronic cards of the level 1.5 trigger (OTC – *Octant Trigger Card*) and those with bigger granularities to the level 1 cards (CCT – *Coarse Centroid Trigger*).

The level 1 cards (CCT), essentially, determine the coincidences at the 3 layers (A, B & C) of the muons system. The criterion is that there should be at least one centroid in each layer and a group of hits compatible with the muons tracks originated from the nominal interaction point is required.

This information is identified, accounted and codified by regions in accordance with certain pre-established global combinations and passed as terms of trigger to the Level 1 general trigger system, as:

- Two muons at the central region ($\eta < 1$).
- One muon at the WAMUS ($\eta < 1.7$).

• **The LAFEX contribution**

At this point, the participation of our group from the LAFEX/CBPF in the implementation of the level 1 muons trigger is worth mentioning.

The work begun on the central region (WAMUS) of the system, in the improvement of the level 1.5 trigger efficiency, through the re-programming of integrated circuits (PLD) of the address cards (MAC).

Later on, the group was responsible for the elaboration and programming of the level 1 coincidence logical equations and for the incorporation of the electronic cards (CCT) in the system modules.

The work of the group culminated with the implementation of the trigger at the regions near to the beam line (SAMUS). At this region, even the cards that receive the centroids (STC) were designed by members of our group.

### 3.4.2 Level Two General Trigger

The last stage of the trigger is constituted of a group of 48 nodes, which are general use computers (VAX station 4000/60), that receive the information from the level 1, *i.e.*, from the digitalization modules (VME) through 8 parallel cables, operating at a 40 Mbytes/s ratio.

If an event that has passed through level 1 satisfies the selection criteria of the level 2, it is transferred from the particular node that have received it to another VAX 6630 type computer that acts as an input and output provider (I/O). This one stores the events in a disk, transfer them to a 8mm type tapes magnetic recorder and keep them available for monitoring through the *workstations*.

During the “1A run”, the typical size of an event was in the range of 500 kbytes and, the amount of collected data in an one year period was around $10^7$ events.

About 10% of the events that are classified as potentially interesting, *i.e.*, with priority for analysis, are sent daily to the so called **express line**. In general, the events are transmitted through an **express line**, at a 1.2

Mbytes/s ratio.

## 3.5 DØ Software

Since the initial proposal of constructing the detector, there was a necessity to develop simulation programs not available in the scientific computer market. Accordingly, since the initial stage of construction, passing through the data acquisition, up to the reconstruction, simulation and analysis of events, it was necessary to utilize an enormous amount of programs generated by the DØ collaboration itself and, thus, a good structuring of the utilized programs was done. Each part of the detector, of the detection process or of the phenomenon that occurs during a $p\bar{p}$ collision, is associated with a certain package of programs.

The package of programs associated with the reconstruction of events, the DØ RECO, transforms the files that contains the rough collected data (as energy deposited in the calorimeter or tracks in the muons chambers) into files that contain the information of an event in terms of physical variables such as locations, energy and momentum.

For each rough data file the reconstruction package generates the **DST**, which contains only physical variables necessary to the subsequent analysis [4] and the type **STA** files that, besides containing the physical variables, store all the rough information (600 kbytes).

[4]Reducing the size of an event to 20 kbytes.

An essential package of programs is the detector simulator, called DØ GEANT, based on Monte Carlo methods. This package simulates the passage of particles through several materials and the interactions occurred as scattering processes. This simulation is fundamental in the pre–analysis of the simulated data, as well as in the preliminary stages of the planning and construction of the detector, and in the development of the reconstruction package code itself.

Another package essential in the integral reconstruction of an event is the trigger simulator (TRIGSIM), which contains all the steps in the trigger logic calculation up to the trigger bits and allows for the determination of the trigger efficiency in the data acquisition process.

The figure 3.8 shows the whole pre–analysis process cycle to which the simulated data generated by the ISAJET are subject. After this stage, a specific process of sample filtering starts. This process consists of the reduction and gathering of data into an adequate format (N-tuples) to be utilized in the analysis stage itself (*off-line* analysis), that was carried out to its large extent by utilizing a PAW package [41]. The analysis work related to this thesis is going to be described in the following chapter.

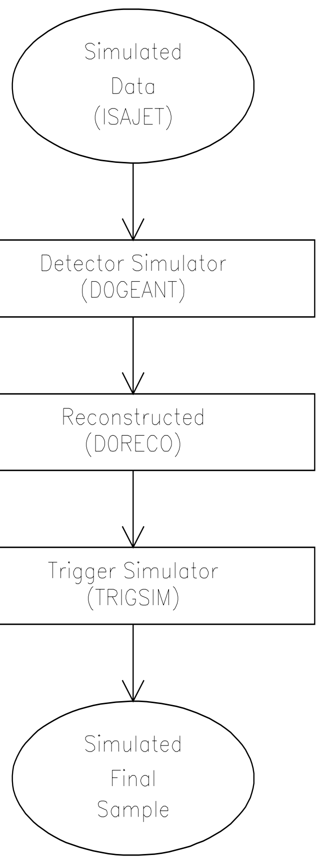


Figure 3.8: Pre-analysis of simulated events.

# Chapter 4

# The Data Analysis : The Inclusive b-Quarks Production Cross Section

The data acquisition process during the “1A run” was developed in a continuous and systematic form. The rate of events that satisfied the muons trigger selection criterion, in general, almost exceeded the capacity of the general trigger and, therefore, it was necessary a pre-scale of the level 1 trigger, so that the transmission to the level 2 trigger could take place at a reasonable rate.

Due to less restrictive requirements than those of the global data run, the muons sample for this analysis work was obtained in special runs (20 in total), when the luminosity of the beam was about $3 \times 10^{30} cm^{-2} s^{-1}$. Still though, in the majority of the cases, the pre-scaling of the trigger was necessary.

After corrections due to the multiple scattering in the calorimeter, microblanking and prescaling, the resulting sample corresponds to an integrated luminosity of 83 $nb^{-1}$ with over 40,000 events stored in tapes.

## 4.1 Selection of Events

The main trigger requirements for the selection of events during the special runs were:

At level 1 : One muon at the central region (WAMUS) of $|\eta| < 1.0$.

At level 2 : One muon at the central region (WAMUS) of $|\eta| < 1.0$. Confirmation of the muon track by the calorimeter. Muon transverse momentum greater than 3 GeV.

## 4.2 Muons Identification

After having obtained the sample of the candidate muons, the reconstruction process started, *i.e.*, the utilization of the DØRECO package. This package identifies candidates muons in three stages:

1 **Choice of hits** : combines rough data (hits, time signals, analog pulses, etc.) with calibration constants to associate them with points in the global coordinates system of the DØ.

2 **Recognition of patterns** : identifies certain groups of hits with a muon track. A preliminary adjustment is carried out and the momentum associated with each track is corrected for the expected mean energy of the muon deposited in the calorimeter.

3 **Global adjustment** : relates a muon track with the appropriate information of the central detector and performs a complete adjustment by the minimum squares method.

These criteria are not sufficient for the complete identification of the muons and, therefore, additional requirements are necessary to characterize the quality of the resulting sample (figure 4.1), *i.e.*, the muons quality.

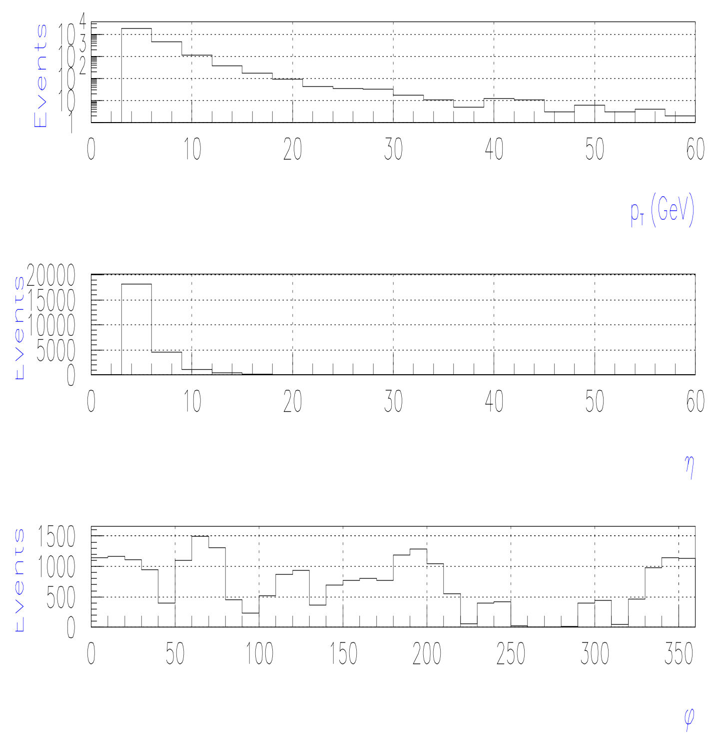


Figure 4.1: Distribution in $p_T$, $\eta$ e $\phi$ of the total reconstructed sample.

## 4.3 Quality of the muons

The criteria that have defined the muons quality of the sample, *i.e.*, the selection criteria (**cuts**) imposed to the data and also applied to the samples obtained by simulation for the determination of the global efficiency were:

- **Confirmation of the calorimeter** : One muon loses in the calorimeter from 1 through 3 GeV of energy. This criteria requires that a muon track be associated with the total energy (ECAL1) deposited in the cells cut by the track, and in its first neighbors, equal or greater than 1 GeV.

- **Magnetic Field Integral** : The muon momentum is calculated by the deviation of its trajectory when it passes through the toroid and through the magnetic field ($\vec{B}$) established in the toroid. This change in the direction is proportional to the integral of the magnetic field along the muon trajectory ($\int \vec{B} \times d\vec{l}$). To ensure a better determination of the momentum and the reduction of the *punchthrough*, a value of $\int \vec{B} \times d\vec{l} \geq 0.6$ GeV was required from the candidates.

- **Tracks synchronism** : An effective criterion for the rejection of cosmic rays is through the determination of the time taken by a muon to pass through the detector, in relation to the collision instant of the beam. One way of performing this determination is to allow the time origins associated with the "hits" (that constitute a track) to vary. The synchronism time ($T_{\o}$) is defined as the one that minimizes the $\chi^2$ test of the track. Cosmic rays are randomic in relation to the collisions. A minimum of 100 $ns$, based on $T_{\o}$ distribution resulting from cosmic rays data, was chosen as the appropriate cut for the rejection of cosmic rays.

- **Confirmation of the central detector** : When crossing the central detector, a good candidate muon leaves a track that can be compared to the track reconstructed by the muons system. The reconstruction code verifies if there is any track in the central detector at a region determined by $\Delta\theta \leq 0.35$ rad e $\Delta\phi \leq 0.35$ rad along the track determined by the muons system.

- **Kinematic cuts** : Some criteria, sometimes redundant with the trigger levels 1 & 2, were required for delimitation of the kinematic domination of the analysis. Only muons with $p_T$ greater than 3 GeV, necessary to pass through the toroids, and smaller than 60 GeV, due to the low statistics and low resolution, and found in the central region at $|\eta| < 0.8$ were accepted. The data distribution according to the azimuthal angle $\phi$ shows deep detection inefficiencies in the region of $80 < \phi < 110^0$. This region is close to the main ring and, therefore, due to the high-tension fluctuations, the efficiencies of the chambers are very low. This region was excluded from this analysis, *i.e.*, good candidate muons must satisfy the cut $\phi \leq 80^0$ e $\phi \geq 110^0$.

- **Impact parameters** : Two parameters were utilized as criteria to define the approximation of the muon track and the collision vertex: the impact parameter 3 D ($I_P$), which is the closest distance between the track and the vertex; and the impact parameter xy ($I_{xy}$), which is the closest distance to the track projection in the plane perpendicular to the beam and the vertex. The cuts associated with these variables were parameterized in accordance with the simulated sample and resulted in:

$$I_P, |I_{xy}| < \sqrt{\left(\frac{300}{p}\right)^2 + 10^2}\ (cm)$$

## 4.4 Efficiencies

In an experiment that involves a complex detector such as the DØ, the experimental results can not be directly compared with the theoretical ones. To perform this comparison, either the "real" data must be "cleaned" from imperfections of the detectors and of inefficiencies on the data processing, or the theoretical results must be submitted to a detailed simulation of the detectors followed by a selection criterion similar to that imposed to the "real" data. By using the second alternative, all the efficiencies obtained from the sample simulation, can be applied to the data.

The basic method for the determination of the various components of the detection efficiency consists of the comparison between the number of events that have passed ($N_P$) and the ones that have not passed ($N_N$) through each one of the muons quality selection criteria (cuts) as per:

$$\epsilon = \frac{N_P}{N_P + N_N}$$

Considering the fact that some inefficiency sources are not well simulated, the detection efficiency associated with a cut can be generally overestimated. On the other hand, the efficiency can be under estimated when calculated from the data themselves, since the data are, in a certain way, contaminated. Anyway, in cases where the determination of a quantity can not be satisfactorily reconstructed and that, after the final cuts the data constitute a reasonably "pure" sample, the efficiencies can be estimated from the data themselves.

The table 4.1 shows the efficiencies related to the cuts of the impact parameter 3D ($I_P$), tracks synchronism ($T_{\o}$) and confirmation of the central detector (NCD), that were determined from the data themselves, and the systematic errors associated with it.

The efficiency associated with the events selection (trigger) and reconstruction processes ($\epsilon_{trig.reco}$), was determined from a muons sample originated from $J/\psi$ decays and was in the range of $0.56 \pm 0.05$ for $p_T^\mu \geq 6$ GeV.

The efficiencies associated with other muons quality criteria, were determined from muons samples originated from simulations, by the ISAJET

| cut | $\epsilon \pm \Delta\epsilon$ |
|---|---|
| $\mathbf{I_P}$ | $0.95 \pm 0.02$ |
| $\mathbf{T}_{\o}$ | $0.89 \pm 0.03$ |
| **NCD** | $0.92 \pm 0.03$ |

Table 4.1: Efficiencies and systematic errors determined from the data.

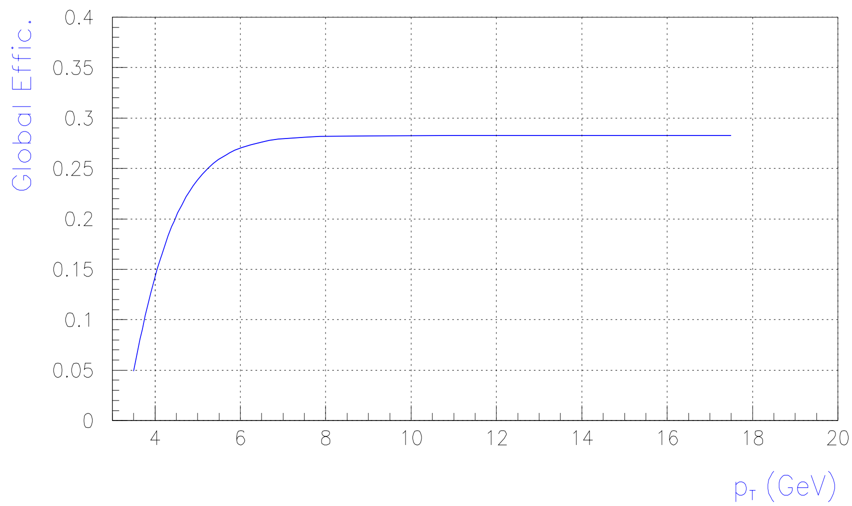


Figure 4.2: Muons detection global efficiency at the region of $|\eta| < 0,8$.

package, of decays from $b$ and $c$-quarks, ($\pi/K$ mesons and $W/Z$ bosons, in a total of over 33,000 events. Such samples were submitted to a complete simulation of the detector (DØGEANT), reconstructed (DØRECO) and submitted to the trigger levels 1 & 2 simulator package (TRIGSIM). The inefficiencies associated with the muons chambers were taken into consideration by the MUSMEAR package.

The data distribution in relation to the pseudo-rapidity (figure 4.1) suggests, clearly, the division of the efficiency determination into three regions:

- $|\eta| < 0.3$
- $0.3 \leq |\eta| \leq 0.7$
- $0.7 \leq |\eta| < 0.8$

Once the efficiencies associated with the cuts of $I_{xy}$, ECAL1 and the $\int \vec{B} \times d\vec{l}$ ($\epsilon_{cuts}$), are determined, at the three regions, the global detection efficiency ($\epsilon_{glob}$) is given by:

$$\epsilon_{glob} = \epsilon_{trig.reco} \times \epsilon_{cuts} \times \epsilon_{I_P} \times \epsilon_{T_0} \times \epsilon_{CD} \times \epsilon_{chamber} \ .$$

This was mediated in $\eta$ and parameterized as a function of $p_T$ (figure 4.2) in such a way that it increases from $0.06\pm0.01$ at $p_T = 3.5$ GeV up to $0.28\pm0.03$ for $p_T > 6.0$ GeV.

The error associated to the efficiency was dominated by uncertainties in the muons chambers efficiencies ($\approx 12\%$).

A total of over 16,000 events that have passed through all the quality cuts, constitute the final muons sample. Its distribution for transverse momentum, pseudo-rapidity and azimuthal angle are shown as histograms in figure 4.3.

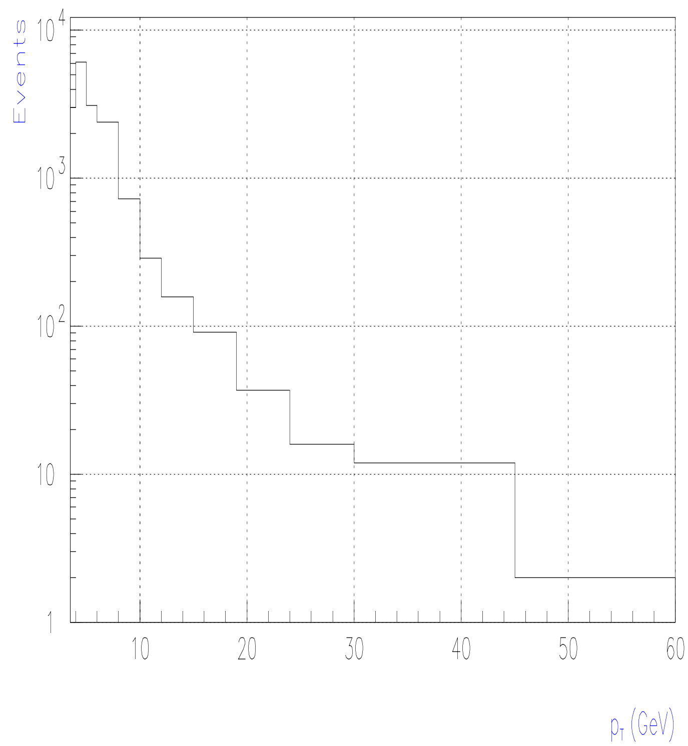


Figure 4.3: $p_T$ spectrum and $\eta$ and $\phi$ distributions of the final muons sample at the central region.

## 4.5 Cosmic Rays Background

After passing through the quality criteria the final sample is reasonably "cleaned" from muons that do not come from $p\bar{p}$ collisions. However, there still persists a small amount of muons originated from cosmic rays. This residual contamination was estimated, through an adjustment of the $T_{\o}$ distribution for the cosmic rays over the data, to be $(9 \pm 3)\%$ and subtracted from the data (figure 4.4).

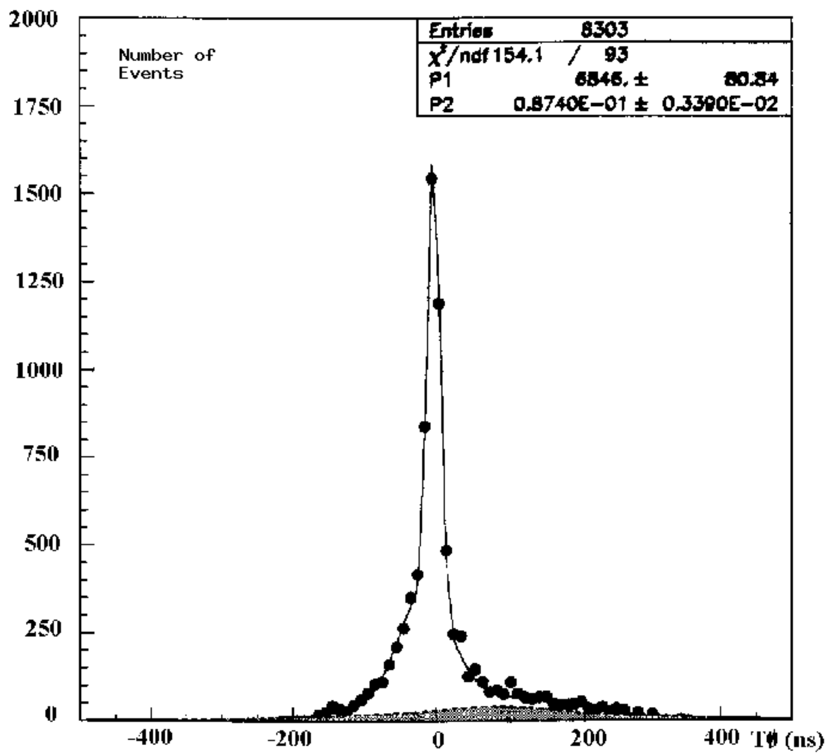


Figure 4.4: Sample and cosmic rays distributions at $T_{\o}$.

## 4.6 Muons Cross Sections

When calculating and representing the transverse momentum spectrum of the inclusive muons production differential cross section, for comparison with the theoretical expectations, two problems appear:

• The first one appears from the necessity to associate each cross section value with a value of $p_T$ at the considered momentum interval. The utilization of variable ranges and the large variation of the spectrum, suggest the utilization of a value of $p_T^w$ as abscissa, that should determine the mean value of the cross section at the considered range [42, 43], *i.e.*:

$$\frac{d\sigma}{dp_T}(p_T^w) = \frac{1}{\Delta p_{T_\imath}} \int_{p_{T_\imath}}^{p_{T_{\imath+1}}} dp_T \; \frac{d\sigma}{dp_T}(p_T) \tag{4.1}$$

where $p_{T_\imath}$ e $p_{T_{\imath+1}}$ are the inferior and superior limits of the $\imath$ of $p_T$, $\Delta p_{T_\imath} = p_{T_{\imath+1}} - p_{T_\imath}$ and $\frac{d\sigma}{dp_T}(p_T)$ is the expected distribution.

• The second one arises from the resolution in the momentum measurement which makes that the observed differential cross section $\frac{d\sigma}{dp_T}(p_T)|_{obs}$ be given by:

$$\frac{d\sigma}{dp_T}(p_T)|_{obs} = \int dp_T \; \mathcal{G}(p_T, p_T') \; \frac{d\sigma}{dp_T'}(p_T')|_{expected} \tag{4.2}$$

*i.e.*, by the convolution of the expected differential cross section $\frac{d\sigma}{dp_T'}(p_T')|_{expected}$ and the resolution function $\mathcal{G}(p_T, p_T')$ that represents the influence of the detector.

Two are the ways for the solution of this problem, either the theoretical cross sections expectations are submitted to a convolution process that was supposedly imposed to the data, or the inverse process of data deconvolution is attempted. The option chosen in this thesis was to do the deconvolution of the data, that also can be carried out through various alternative ways [34, 44].

The essence of the utilized method, called **bayesian method**, consists in a probabilistic interpretation of the problem.

∘ The bayesian method

The resolution function is a gaussian one adjusted from the data, and it is expressed in terms of the inverse of the momentum, with width $\sigma(1/p)$ (figure 4.5).

The adjustment function for the width is given by:

$$\frac{\sigma(1/p)}{1/p} = \sqrt{[0.18\,(1-2/p)]^2 + (0.008p)^2} \tag{4.3}$$

Writing down

$$\begin{cases} x = 1/p \\ y = 1/p' \end{cases}$$

the convolution and deconvolution can be described as

$$\begin{cases} n(y) = \int dx \;\, P(y,x)n(x) \\ n(x) = \int dy \;\, P(x,y)n(y) \end{cases}$$

where $n(x)$ is the expected spectrum, $n(y)$ is the observed spectrum, $P(y,x)$ is the probability of occurrence of $y$ if $x$ occurred and $P(x,y)$ is the probability of occurrence of $x$ if $y$ occurred.

The method consists on the obtention, through an iterative process, of the $P(x,y)$ probability from $P(x,y)$ and of the probability of occurrence of

$x$ $(P(x,y))$, utilizing the so called Bayes theorem [45], that can be expressed by:

$$P(x,y) \propto P(x)\ P(y,x)$$

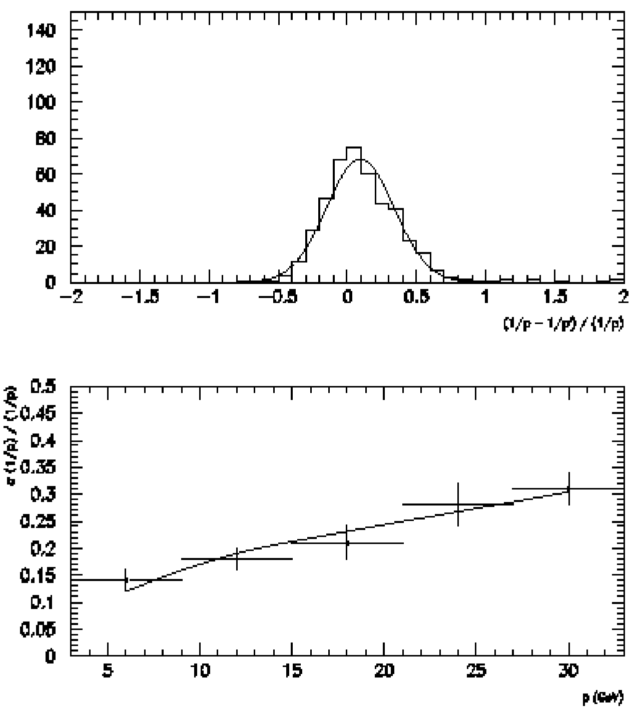


Figure 4.5: Adjustments of the resolution function at $15 < p_T < 21$ GeV range and of the momentum resolution (width) at $3 < p_T < 33$ GeV range.

• **Inclusive Muons Production**.

The muons production differential cross section, determined according to the equation 2.9, is shown in figure 4.6. The dashed curves represent the expected contributions from decays of $\pi/K$ mesons and $W/Z$ bosons. The difference between the sum of the contributions from $\pi/K$ mesons &

$W/Z$ bosons and the experimental points is attributed to the decays of $b$ & $c$-quarks.

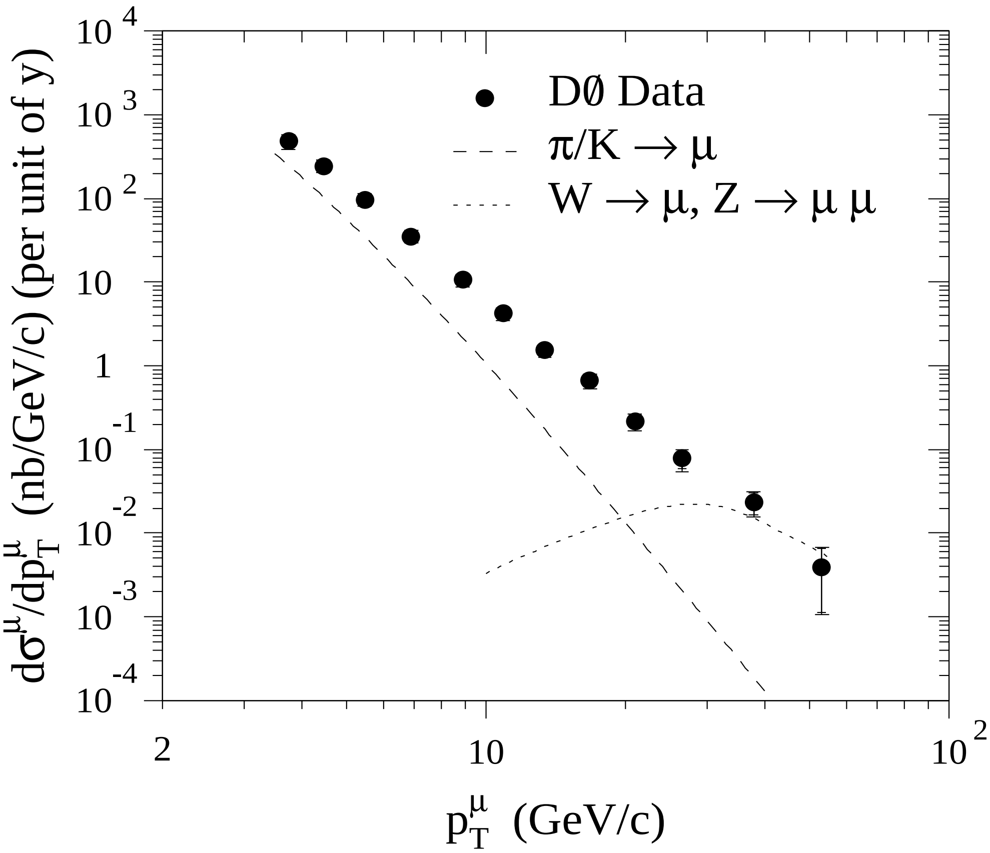


Figure 4.6: Comparison between the muons inclusive cross section with the expected contributions from decays of $\pi/K$ mesons and $W/Z$ bosons.

The observed distribution is consistent with the fact, already well established, of the great contribution of the $\pi/K$ mesons decays, at low values of $p_T$, and of the domination of $W/Z$ bosons decays, at high $p_T$.

This consistency is important for the verification of the sample cross section normalization.

The $W/Z$ bosons decays were simulated by the ISAJET package, with cross sections and systematic errors checked with data from the $W/Z$ bosons study group [46], also from the DØ collaboration.

The table 4.2 shows the measured values of the inclusive muons production cross sections at the central region of the DØ detector and the associated errors.

| $p_T$ (GeV) range | $p_T^\mu$ (GeV) | $d\sigma/dp_T$ (nb/GeV) | stat. error | sist. error | total error |
|---|---|---|---|---|---|
| 3,5–4 | 3.7 | 485.0 | 0.018 | 0.20 | 0.20 |
| 4–5 | 4.5 | 245.2 | 0.013 | 0.17 | 0.17 |
| 5–6 | 5.5 | 97.8 | 0.018 | 0.17 | 0.17 |
| 6–8 | 6.9 | 35.5 | 0.020 | 0.16 | 0.16 |
| 8–10 | 8.9 | 10.6 | 0.037 | 0.16 | 0.16 |
| 10–12 | 10.9 | 4.2 | 0.059 | 0.16 | 0.17 |
| 12–15 | 13.4 | 1.5 | 0.08 | 0.16 | 0.18 |
| 15–19 | 16.8 | 0.66 | 0.12 | 0.16 | 0.19 |
| 19–24 | 21.0 | 0.22 | 0.16 | 0.16 | 0.23 |
| 24–30 | 26.5 | 0.078 | 0.25 | 0.16 | 0.30 |
| 30–45 | 37.8 | 0.023 | 0.29 | 0.16 | 0.33 |
| 45–60 | 53.0 | 0.004 | 0.71 | 0.16 | 0.72 |

Table 4.2: Inclusive muons production cross section of pair $|\eta| < 0.8$.

• **Muons from b-quarks decays**.

Due to the statistics problems for high values of $p_T$ and due to the great contribution from the decays of $\pi/K$ mesons at low values of $p_T$ ($\approx 25$ %), the inclusive production cross section of muons originated from $b$-quarkswas determined (equation 2.10) at the $p_T$ range 4-30 GeV.

After estimating and subtracting the contribution from $W/Z$ bosons decays ($N^{\mu}_{W/Z}$) of the muons sample, it is expected that the excess is mainly originated from $b$ & and $c$-quarks.

The determination of the fraction of muons from $b$-quarks ($f_b$) was carried out by utilizing the muon transverse momentum ($p_T^{rel}$) in relation to the associated jet.

Jets are reconstructed for $E_T^{jet} > 8$ GeV, using the cone algorithm [18] with radius $R = 0.7$ in the pseudorapidity *versus* azimuthal angle space. Once the accompanying jets of muons from semi-leptonic decays have low transverse energy, only 60 % of the muons have a jet nearby ($\Delta R^{\mu,jet} < 1$). This percentage is consistent with the reconstructed jet fraction in simulated events and, therefore, it is assumed that the final distributions of the muons sample with or without the requirement of jets, are similar.

Accordingly, the fraction $f_b$ extracted from the subset of muons with associated jets, supposedly, is the same as for the muons sample without jets.

The distributions relative to the decays of $b$-quarks, $c$-quarks and $\pi/K$

mesons were obtained through simulations with the ISAJET package. The $b$-quarks decays simulation includes the directly decay ($b \rightarrow \mu$) and the sequential one ($b \rightarrow c \rightarrow \mu$) with the adequate branching ratios [47]. The resulting spectrum has, practically, the same shape of the leptons spectrum measured by the OPAL collaboration [48] at the LEP.

The figure 4.7 shows the $p_T^{rel}$ distribution for the $p_T$ range 8-30 GeV.

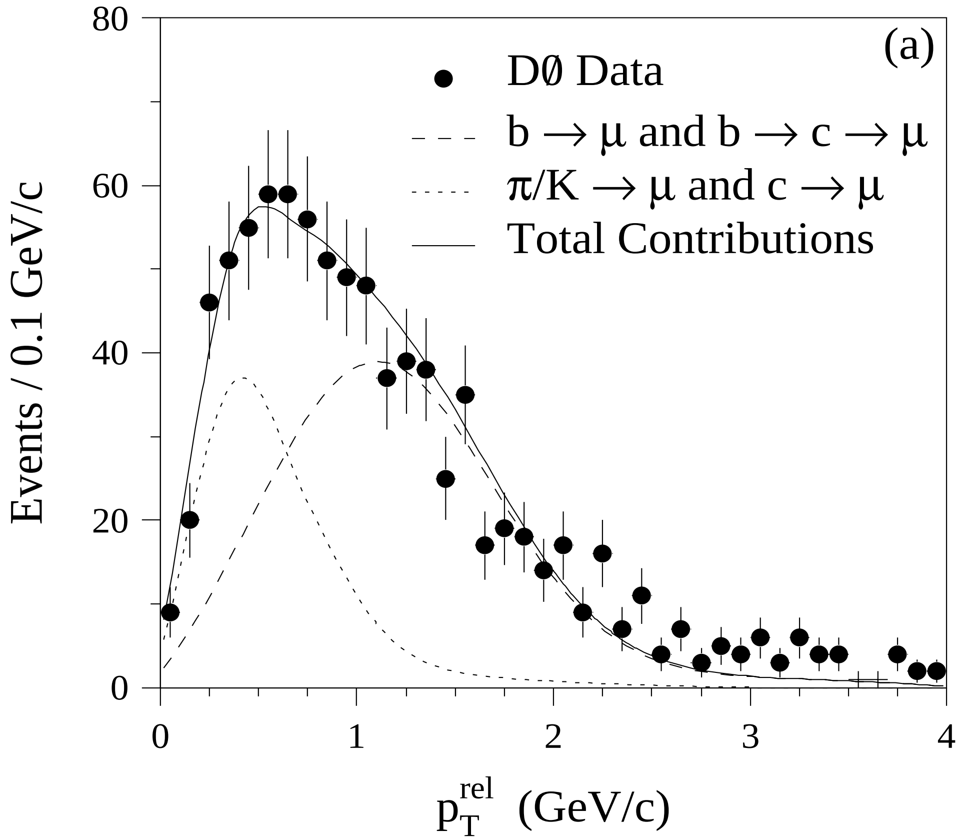


Figure 4.7: $p_T^{rel}$ distribution for the subset of muons associated with jets in $p_T$ range 8-30 GeV.

Finally, the fraction $f_b$ was determined by adjustments of the $p_T^{rel}$ distribution of $b$-quarks, $c$-quarks and $\pi/K$ mesons at $p_T$ range (figure 4.8. The errors on the fraction $f_b$ were estimated in 12 %.

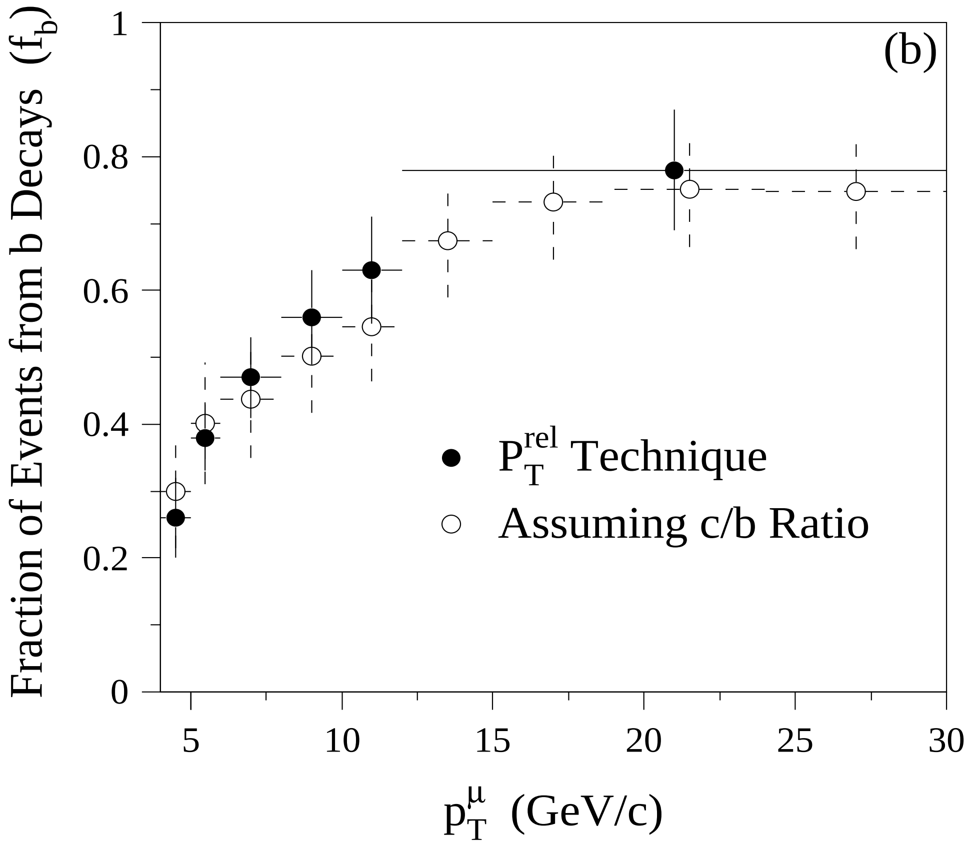


Figure 4.8: The $f_b$ fraction as a function of $p_T$. The solid points are from the $p_T^{rel}$ fitting technique and the open circles are from the $c/b$ ratio method.

This result was verified, through another way, by the subtraction of the expected decays from $\pi/K$ mesons and $W/Z$ bosons from the data sample and, by using the $c/b$ ratio of the expected *charm* and *bottom* contributions. The error for this method was estimated varying this ratio by 50 %.

The term $f_p$ in the equation 2.10 is the correction factor due to the momentum measurement resolution and, was determined by the bayesian method. It varies from 1, at low $p_T$, through 0.7 for $p_T = 20$ GeV. The uncertainty in this factor ($\approx 6$ %) was estimated by varying the resolution function according to its errors.

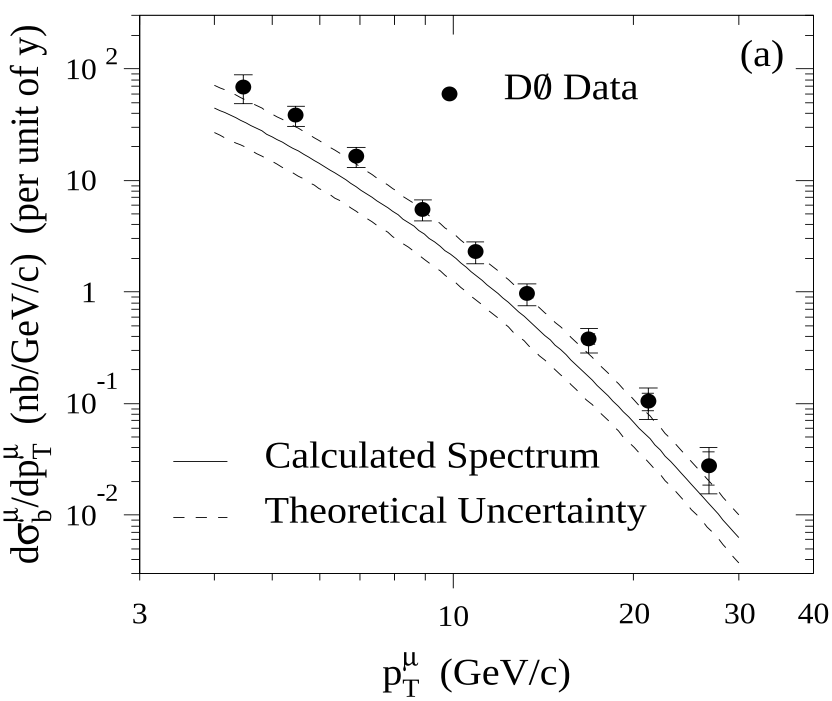


Figure 4.9: Muons spectrum for $b$-quarks inclusive decays.

The resulting experimental spectrum is shown in figure 4.9. The theoretical expectation, also shown in the figure 4.9, was calculated using the ISAJET [1] for the $b$-quarks production, fragmentation and decay, with the cross section normalized by calculation at perturbative NLO QCD [14].

The table 4.3 shows the measured values of the inclusive production cross section of muons originated from $b$-quarks decays. This result was obtained without any hypothesis related to $p\bar{p}$ collision stages that involve non-perturbative processes such as the hadronization. And, considering the theoretical and experimental uncertainties, it is a result well described by the expected contribution from various sources.

| $p_T$ (GeV) range | $p_T^{\mu}$ (GeV) | $d\sigma/dp_T$ (nb/GeV) | stat. error | sist. error | total error |
|---|---|---|---|---|---|
| 4–5 | 4.5 | 68.3 | 0.013 | 0.29 | 0.29 |
| 5–6 | 5.5 | 38.4 | 0.018 | 0.21 | 0.21 |
| 6–8 | 6.9 | 16.4 | 0.020 | 0.21 | 0.21 |
| 8–10 | 8.9 | 5.5 | 0.037 | 0.21 | 0.21 |
| 10–12 | 10.9 | 2.3 | 0.059 | 0.21 | 0.22 |
| 12–15 | 13.4 | 0.97 | 0.080 | 0.21 | 0.22 |
| 15–19 | 16.8 | 0.38 | 0.11 | 0.23 | 0.25 |
| 19–24 | 21.2 | 0.11 | 0.18 | 0.26 | 0.32 |
| 24–30 | 26.7 | 0.028 | 0.33 | 0.30 | 0.44 |

Table 4.3: Muons spectrum for $b$-quarks inclusive decays at the region $|y| < 0.8$.

[1] See section 2.3.

## 4.7 b-quark production cross section

Using the process described in section 2.6, the ratio between the cross sections

$$\left(\frac{\sigma^b}{\sigma^\mu}\right)_{ISAJET}$$

depends on the shape of the $p_T$ spectrum but not on the normalization. The 12 %uncertainty in the spectrum shape was estimated by replacing the MRSDØ partonic distributions with MRSD [49].

The error in the Peterson parameter $\epsilon_b$ together with a variation of $1\sigma$ in the branching ratio of the $B$ mesons decays was estimated in 13 %. By adding the muons cross section error, the systematic uncertainty resulting in the $b$-quarks cross section was 27 %.

The figure 4.10 shows the final result of this thesis, the inclusive $b$-quarks production cross section as a function of $p_T^{min}$ in the rapidity range of $|y| < 1$. The curves represent the QCD and NLO predictions [14] using the MRSDØ partonic distribution functions. Results from the CDF for the inclusive leptons production[35] are also shown for subsequent comparisons.

The table 4.4 shows the values calculated from the inclusive $b$-quarks production cross sections at the central region of the DØ detector.

The final comments, comparisons with other results and conclusions related to these results are the subject of the next chapter of conclusion of this thesis.

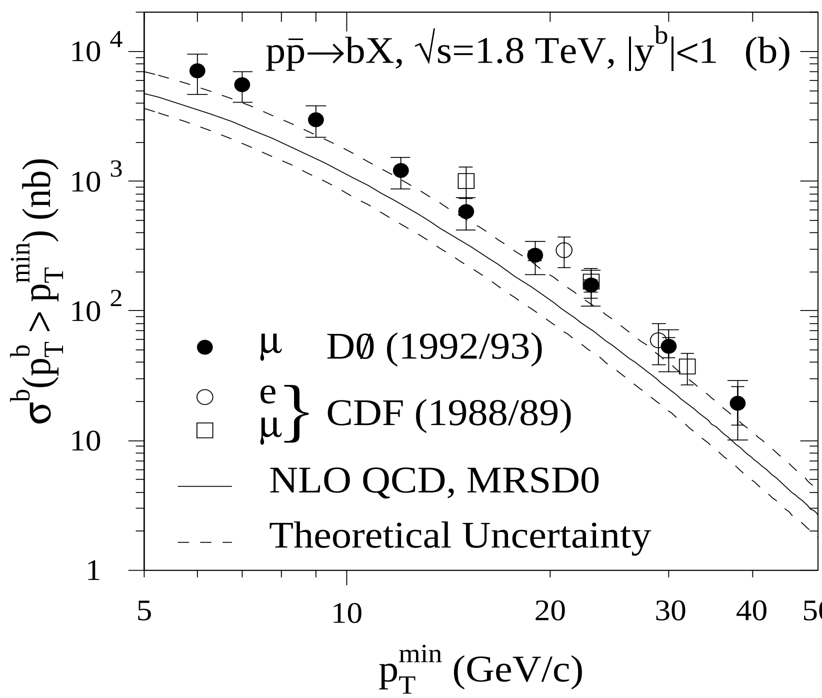


Figure 4.10: Inclusive $b$-quarks production cross section compared to NLO QCD predictions.

| $p_T^{min}$ (GeV) | $\sigma^b$ (nb) | stat. error | sist. error | total error |
|---|---|---|---|---|
| 6 | 7104.2 | 0.013 | 0.34 | 0.34 |
| 7 | 5533.5 | 0.018 | 0.27 | 0.27 |
| 9 | 2987.8 | 0.020 | 0.27 | 0.27 |
| 12 | 1204.4 | 0.037 | 0.27 | 0.27 |
| 15 | 585.0 | 0.059 | 0.27 | 0.28 |
| 19 | 266.2 | 0.080 | 0.27 | 0.28 |
| 23 | 157.2 | 0.11 | 0.29 | 0.31 |
| 30 | 53.0 | 0.18 | 0.31 | 0.36 |
| 38 | 19.5 | 0.33 | 0.35 | 0.48 |

Table 4.4: Inclusive $b$-quarks production cross sections.

# Chapter 5

# Conclusions and Perspectives

The hadronic collisions at the energies reached in the Tevatron of the Fermilab allow for the production of heavy quarks like the $b$ (*bottom*) and the $t$ (*top*), and, therefore, constitute an interesting source of investigation on the nature of the production mechanisms of these quarks through strong interactions.

The production, detection and reconstruction of events that indicate the presence of heavy quarks involve various experimental difficulties. Only recently the production of the top quark was possible. The first experimental measurements of the $b$-quarks production cross sections, at energy and pseudo-rapidity ranges comparable to the ones utilized by the DØ collaboration, were carried out by the CDF and did not agree with the QCD predictions. On the other hand, previous measurements at lower energy regions carried out by the UA1 collaboration, were in well agreement with the QCD predictions. The challenge to understand the source of this discrepancy was one of the main motivations of this work, which purpose was the determination of the inclusive b-quarks production cross section at a wider kinematic region than that involved in previous measurements.

The DØ detector, by having the characteristics necessary for the observation of events related to the heavy quarks production, was chosen by the LAFEX group for its first integration in a colliding rings experiment. At the time of acceptance of the group by the other members of the DØ collaboration, the detector was still not in operation, what have allowed the group to have an important participation in the implementation of the detector as an active instrument of observation and measurement of phenomena occurring at high energies.

Another characteristic of the DØ detector is the great angular coverage in relation to the $p\bar{p}$ beam line, greater than any other detector in operation in colliding rings. The detector division in pseudo-rapidity ranges reveals that at least 3 distinct regions have special detection characteristics. Based on that, the analysis performed in this thesis concentrated in only one of these regions (the central region).

Undoubtedly, the DØ detector will allow, up to the end of this century, for the carrying out of various $p\bar{p}$ collisions experiments at the Tevatron, in an energy scale unachievable by any other laboratory.

The data acquisition analysed in this thesis is due to a direct participation of the LAFEX group in the muons trigger system, and has allowed for the determination of the inclusive muons production cross section measurement, from which the inclusive $b$-quarks production cross section was determined. The results, agree, within the experimental errors (figure 4.10), with the new results presented by the CDF collaboration [35] from their measurements of inclusive leptons production. Other results from the CDF collaboration, that showed some discrepancies in the spectrum at low values of $p_T$, derive from analysis based on final states different[1] than those utilized in this analysis. Previous results, from the UA1 collaboration [30], obtained at $\sqrt{s} = 630$ GeV, at the low $p_T$ region, also agree with the ones of this thesis.

The results presented herein also indicate that the NLO QCD description for the heavy quarks production in $p\bar{p}$ collisions at $\sqrt{s} = 1.8$ TeV is adequate for the studied kinematic range $|y| < 1$ and $p_T > 6$ GeV, within the theoretical uncertainties (figure 4.10).

The results obtained in this thesis were, as already mentioned, also important for increasing the number of observation events of the top quark, since this one necessarily decays into a $b$-quark. In particular, the channel which subsequent $b$-quark decay is given by,

$$t \to bX \to \mu X$$

utilizes selection criteria similar to the ones utilized in this thesis.

As for the perspectives of future experimental works of the group,

[1] $J/\psi$ or exclusive decays of $b \to c$

related to the bottom production, it is necessary that the rapidity region be increased, *i.e.*, regions closer to the beam need to be explored. In order to achieve this objective, it is important to have a modification in the detector, that would allow for the reduction in the noise level at these regions. For this purpose, the LAFEX group is already engaged in a modification work of the electronics associated with the muons system. This will help to increase the measured rapidity range. By this way, results related to the next run ("run 2") will allow for the establishment of the cross section dependence in relation to the rapidity, *i.e.*, for the determination of $d\sigma/dy$. It is expected then, that this new result can be used to improve the parametrization of the gluonic distributions.

# Appendix A

# DØ Colaboration

S. Abachi[9], B. Abbott[27], M. Abolins[19], B.S. Acharya[33], I. Adam[8], D.L. Adams[28], M. Adams[13], S. Ahn[9], H. Aihara[16], G. Alvarez[14], G.A. Alves[6], N. Amos[18], E.W. Anderson[15], Yu. Antipov[26], S.H. Aronson[3], R. Astur[31], R.E. Avery[23], A. Baden[17], V. Balamurali[24], J. Balderston[12], B. Baldin[9], J. Bantly[4], J.F. Bartlett[9], K. Bazizi[5], T. Behnke[31], J. Bendich[16], S.B. Beri[25], V. Bezzubov[26], P.C. Bhat[9], V. Bhatnagar[25], N. Biswas[24], G. Blazey[29], S. Blessing[23], A. Boehnlein[35], F. Borcherding[9], J. Borders[29], N. Bozko[26], A. Brandt[9], R. Brock[19], A. Bross[9], D. Buchholz[23], V. Burtovoi[26], J.M. Butler[9], O. H. Callot[31], H. Castilla-Valdez[7], D. Chakraborty[31], S. Chekulaev[26], J. Chen[2], L. P. Chen[16], W. Chen[31], L. Chevalier[30], S. Chopra[25], B.C. Choudhary[5], J. H. Christenson[9], M. Chung[13], D. Claes[31], A.R. Clark[16], W.G. Cobau[17], J. Cochran[31], W.E. Cooper[9], C. Cretsinger[29], D. Cullen-Vidal[4], M. Cummings[12], J.P. Cussonneau[30], D. Cutts[4], O.I. Dahl[16], K. De[34], M. Demarteau[9], R. Demina[21], K. Denisenko[9], N. Denisenko[9], D. Denisov[32], S. Denisov[26], W. Dharmaratna[11], H.T. Diehl[9], M. Diesburg[9], R. Dixon[9], P. Draper[34], Y. Ducros[30], S. Durston-Johnson[29], D. Eartly[9], D. Edmunds[19], A. Efimov[26], J. Ellison[5], V.D. Elvira[9], R. Engelmann[31], G. Eppley[28], O. Eroshin[26], V. Evdokimov[26], S. Fahey[19], G. Fanourakis[29], M. Fatyga[3], M.K. Fatyga[29], J. Featherly[3], S. Feher[31], D. Fein[2], T. Ferbel[29], G. Finocchiaro[31], H.E. Fisk[9], E. Flattum[19], G.E. Forden[2], M. Fortner[22], P. Franzini[8], S. Fredriksen[32], S. Fuess[9], C.S. Gao[9], T.L. Geld[32], K. Genser[9], C.E. Gerber[9], B. Gibbard[3], V. Glebov[32], J.F. Glicenstein[30], B. Gobbi[23], M. Goforth[11], A. Goldschmidt[16], B. Gomez[1], M.L. Good[31], H. Gordon[3], N. Graf[3], P.D. Grannis[31], D.R. Green[9], J. Green[22], H. Greenlee[9], N. Grossman[19],

P. Grudberg[16], S. Grünendahl[29], J.A. Guida[31], J.M. Guida[3], W. Guryn[3], N.J. Hadley[17], H. Haggerty[9], S. Hagopian[11], V. Hagopian[11], R.E. Hall[5], S. Hansen[9], J.M. Hauptman[15], D. Hedin[22], A.P. Heinson[5], U. Heintz[8], T. Heuring[11], R. Hirosky[29], B. Hoeneisen[1], J.S. Hoftun[4], T. Hu[31], J.R. Hubbard[30], T. Huehn[5], S. Igarashi[9], A.S. Ito[9], E. James[2], J. Jaques[24], J.Z.Y. Jiang[31], T. Joffe-Minor[23], K. Johns[2], M. Johnson[9], H. Johnstad[32], A. Jonckheere[9], M. Jones[12], H. Jöstlein[9], C.K. Jung[31], S. Kahn[3], R. Kehoe[24], M. Kelly[24], A. Kernan[5], L. Kerth[16], A. Kholodenko[26], A. Kiryunin[26], E. Kistenev[26], A. Klatchko[11], B. Klima[9], B. Klochkov[26], C. Klopfenstein[31], V. Klyukhin[26], V. Kochetkov[26], J.M. Kohli[25], D. Koltick[27], J. Kotcher[32], I. Kotov[26], J. Kourlas[20], A. Kozelov[26], E. Kozlovsky[26], M.R. Krishnaswamy[33], S. Krzywdzinski[9], S. Kunori[17], S. Lami[31], G. Landsberg[31], R.E. Lanou[4], J. Lee-Franzini[31], H. Li[31], J. Li[34], R.B. Li[9], Q.Z. Li-Demarteau[9], J.G.R. Lima[6], S.L. Linn[11], J. Linnemann[19], R. Lipton[9], Y.C. Liu[23], F. Lobkowicz[29], P. Loch[2], S.C. Loken[16], S. Lokos[31], L. Lueking[9], A.K.A. Maciel[6], R.J. Madaras[16], R. Madden[11], Ph. Mangeot[30], I. Manning[9], B. Mansoulié[30], H.S. Mao[9], S. Margulies[13], R. Markeloff[22], L. Markosky[2], T. Marshall[14], H.J. Martin[14], M.I. Martin[9], P.S. Martin[9], M. Marx[31], B. May[2], A. Mayorov[26], R. McCarthy[31], T. McKibben[13], J. McKinley[19], X.C. Meng[9], K.W. Merritt[9], H. Miettinen[28], A. Milder[2], C. Milner[32], A. Mincer[20], N.K. Mondal[33], H.E. Montgomery[9], P. Mooney[19], M. Mudan[20], C. Murphy[14], C.T. Murphy[9], F. Nang[4], M. Narain[9], V.S. Narasimham[33], H.A. Neal[18], J.P. Negret[1], P. Nemethy[20], D. Nešić[4], D. Norman[17], L. Oesch[18], V. Oguri[6], E. Oltman[16], N. Oshima[9], D. Owen[19], M. Pang[15], A. Para[9], C.H. Park[9], R. Partridge[4], M. Paterno[31], A. Peryshkin[9], M. Peters[12], B. Pi[19], H. Piekarz[11], Yu. Pischalnikov[26], D. Pizzuto[31], A. Pluquet[30], V. Podstavkov[26], B.G. Pope[19], H.B. Prosper[11], S. Protopopescu[3], Y.K. Que[9], P.Z. Quintas[9], G. Rahal-Callot[31], R. Raja[9], S. Rajagopalan[31], M.V.S. Rao[33], L. Rasmussen[31], A.L. Read[9], S. Repond[22], S. Reucroft[21], V. Riadovikov[26], M. Rijssenbeek[31], N.A. Roe[16], P. Rubinov[31], R. Ruchti[24], J. Rutherfoord[2], A. Santoro[6], L. Sawyer[34], R.D. Schamberger[31], D. Schmid[32], J. Sculli[20], A. Shkurenkov[26], M. Shupe[2], J.B. Singh[25], V. Sirotenko[22], J. Skeens[28], W. Smart[9], A. Smith[2], D. Smith[5], R.P. Smith[9], G.R. Snow[18], S. Snyder[31], J. Solomon[13], P.M. Sood[25], M. Sosebee[34], M. Souza[6], A.L. Spadafora[32], R. Stephens[10], M.L. Stevenson[16], D. Stewart[18], F. Stocker[32], D. Stoyanova[26], K. Streets[17], M. Strovink[16], A. Suhanov[26], A. Taketani[9], M. Tartaglia[9], J. Teiger[30], J. Thompson[31], T.G. Trippe[16], P.M. Tuts[8], P.R. Vishwanath[33], A. Volkov[26], A. Vorobiev[26], H.D. Wahl[11], D.C. Wang[9], L.Z. Wang[9], J. Warchol[24],

M. Wayne[24], H. Weerts[19], W.A. Wenzel[16], A. White[34], J.T. White[35], J.A. Wightman[35], J. Wilcox[21], S. Willis[22], S.J. Wimpenny[5], Z. Wolf[10] J. Womersley[32], D.R. Wood[9], Y. Xia [19], D. Xiao[11], P.P. Xie[9], H. Xu[4], R. Yamada[9], P. Yamin[3], C. Yanagisawa[31], J. Yang[20], M.J. Yang[9], T. Yasuda[21], C. Yoshikawa[12], S. Youssef[11], J. Yu[31], C. Zeitnitz[2], S. Zhang[18], Y.H. Zhou[9], Q. Zhu[20], Y.S. Zhu[9], D. Zieminska[14], A. Zieminski[14], A. Zinchenko[15], A. Zylberstejn[30]

# Institutions

[1]Universidad de los Andes, Bogota, Colombia
[2]University of Arizona, Tucson, Arizona 85721
[3]Brookhaven National Laboratory, Upton, New York 11973
[4]Brown University, Providence, Rhode Island 02912
[5]University of California, Riverside, California 92521
[6]LAFEX, Centro Brasileiro de Pesquisas Físicas, Rio de Janeiro, Brasil
[7]CINVESTAV, Mexico City, Mexico
[8]Columbia University, New York, New York 10027
[9]Fermi National Accelerator Laboratory, Batavia, Illinois 60510
[10]University of Florida, Gainesville Florida 32611
[11]Florida State University, Tallahassee, Florida 32306
[12]University of Hawaii, Honolulu, Hawaii 96822
[13]University of Illinois, Chicago, Illinois 60680
[14]Indiana University, Bloomington, Indiana 47405
[15]Iowa State University, Ames, Iowa 50011
[16]Lawrence Berkeley Laboratory, Berkeley, California 94720
[17]University of Maryland, College Park, Maryland 20742
[18]University of Michigan, Ann Arbor, Michigan 48109
[19]Michigan State University, East Lansing, Michigan 48824
[20]New York University, New York, New York 10003
[21]Northeastern University, Boston, Massachusetts 02115
[22]Northern Illinois University, DeKalb, Illinois 60115
[23]Northwestern University, Evanston, Illinois 60208
[24]University of Notre Dame, Notre Dame, Indiana 46556
[25]University of Panjab, Chandigarh 16-00-14, India
[26]Institute for High Energy Physics, 142-284 Protvino,Russia
[27]Purdue University, West Lafayette, Indiana 47907
[28]Rice University, Houston, Texas 77251

[29]University of Rochester, Rochester, New York 14627
[30] DAPNIA-CE Saclay, F-91191 Gif-sur-Yvette, France
[31]State University of New York, Stony Brook, New York 11794
[32]SSC Laboratory, Dallas, Texas 75237
[33]Tata Institute of Fundamental Research, Colaba, Bombay 400-005, India
[34]University of Texas, Arlington, Texas 76019
[35]Texas A&M University, College Station, Texas 77843

# Appendix B

# Rapidity and Lorentz Transformations

The rapidity ($y$), defined by:

$$y = \frac{1}{2}\ log\ \left(\frac{E + p_L}{E - p_L}\right)$$

where $E$ is the energy of a particle resulting from a $p\bar{p}$ collision and $p_L$ is the projection of its momentum at the $p\bar{p}$ beam direction, seems not to be related to the Lorentz transformations. However, for a Lorentz boost in the $p\bar{p}$ beam direction, between a referential $S$ and a $S'$, while the transversal component ($p_T$) of the momentum is invariable, the longitudinal components ($p_L$ and $p'_L$) and the energies ($E$ and $E'$) are related by

$$\begin{cases} p_L = \gamma(p'_L + \beta E) \\ E = \gamma(E' + \beta p'_L) \end{cases}$$

where $\beta$ is the speed of a referential in relation to the other, and

$$\gamma = \frac{1}{\sqrt{1-\beta^2}}$$

is the so called Lorentz factor.

Considering that $\gamma^2 - (\gamma\beta)^3 = 1$, a parameter $y$ can be defined by:

$$\begin{cases} coshy = \gamma \\ senhy = (\gamma\beta) \end{cases}$$

Accordingly, a boost of Lorentz can be described as

$$\begin{cases} E \;\; = E' coshy + p'_L senhy \\ p_L = E' senhy + p'_L coshy \end{cases}$$

or, in a matrix notation as

$$\begin{pmatrix} E \\ p_L \end{pmatrix} \begin{pmatrix} coshy & senhy \\ senhy & coshy \end{pmatrix} \begin{pmatrix} E' \\ p'_L \end{pmatrix}$$

that can also be written as

$$P = (coshy\ \mathcal{I} + sinhy\ \mathcal{K})\ P'$$

where $P = \begin{pmatrix} E \\ p_L \end{pmatrix}$ $\qquad P' = \begin{pmatrix} E' \\ p'_L \end{pmatrix}$

$\mathcal{I} = \begin{pmatrix} 1 & 0 \\ 0 & 1 \end{pmatrix}$ $\qquad \mathcal{K} = \begin{pmatrix} 0 & 1 \\ 1 & 0 \end{pmatrix}$

Considering that $\mathcal{K}^2 = \mathcal{I}$ and

$$
\begin{aligned}
e^{y\mathcal{K}} &= \mathcal{I} + (y\mathcal{K}) + \frac{(y\mathcal{K})^2}{2} + \frac{(y\mathcal{K})^3}{3!} + \dots \\
e^{y\mathcal{K}} &= \underbrace{\left(1 + \frac{y^2}{2} + \dots\right)}_{cosh\ y} \mathcal{I} + \underbrace{\left(y + \frac{y^3}{3!} + \dots\right)}_{senh\ y} \mathcal{K}
\end{aligned}
$$

the boost of Lorentz can be concisely written as

$$P = e^{y\mathcal{K}}\ P'.$$

If $S'$ is a referential such that $p'_L = 0$,

$$\begin{cases} E = \gamma E' = E' coshy = \frac{E'}{2}(e^y + e^{-y}) \\ p_L = \gamma\beta E' = E' senhy = \frac{E'}{2}(e^y - e^{-y}) \end{cases}$$

$$\Downarrow$$

$$e^y = \frac{E + p_L}{E'}$$

$$\Downarrow$$

$$e^{2y} = \frac{(E + p_L)^2}{E'^2}$$

e $M$ is the mass of the particle

$E'^2 = M^2 + p'^2_T = M^2 + p^2_T = E^2 - (p^2_T + p^2_L) + p^2_T = E^2 - p^2_L = (E + p_L)(E - p_L)$

$$\Downarrow$$

$$e^{2y} = \frac{E + p_L}{E - p_L} \qquad \Rightarrow \qquad y = \frac{1}{2}\ log\ \left(\frac{E + p_L}{E - p_L}\right)$$

*i.e.*, the parameter that describes a boost of Lorentz can be associated with the rapidity of a particle.

For any boost in the $p\bar{p}$ beam direction,

$$\begin{cases} E + p_L = (\gamma + \beta)(E' + p'_L) \\ E - p_L = (\gamma - \beta)(E' - p'_L) \end{cases}$$

$$\Downarrow$$

$$\begin{aligned} y &= \frac{1}{2}\ log\ \left[\frac{\gamma + \beta}{\gamma - \beta} \times \frac{E' + p'_L}{E' - p'_L}\right] \\ y &= \underbrace{\frac{1}{2}\ log\ \left(\frac{E' + p'_L}{E' - p'_L}\right)}_{y'} + \underbrace{\frac{1}{2}\ log\ \left(\frac{\gamma + \beta}{\gamma - \beta}\right)}_{constant} \\ y &= y' + constant \end{aligned}$$

considering that in the collision regimen of the Tevatron $\beta \approx 1$ , *i.e.*, $\gamma \gg 1$

$$y \approx y'$$

• **Limit at high energies**

Considering that $p_L = |\vec{p}| \cos\theta$, if the energy of a particle is much greater than its mass ($E \gg m$)

$$E \approx |\vec{p}|$$

In this case, the rapidity can be written as

$$
\begin{aligned}
y &\approx \frac{1}{2}\, log\ \left(\frac{|\vec{p}| + |\vec{p}|\cos\theta}{|\vec{p}| - |\vec{p}|\cos\theta}\right) \\
y &\approx \frac{1}{2}\, log\ \left(\frac{1 + \cos\theta}{1 - \cos\theta}\right) \\
y &\approx \frac{1}{2}\, log\ \left(\frac{cos^2\theta/2}{sin^2\theta/2}\right) \\
y &\approx log\ |cotg\theta/2| \\
y &\approx log\ |tan\theta/2| \\
y &\approx \eta
\end{aligned}
$$

*i.e.*, the rapidity tends to pseudo–rapidity.

In table B.1, some typical values of pseudo–rapidity and their corresponding polar angles are shown.

| $\eta$ | $\theta$ ($^0$) |
|---|---|
| 0,8 | 48,4 |
| 1,0 | 40,3 |
| 1,2 | 33,5 |
| 2,4 | 10,36 |
| 3,6 | 3,10 |
| 4,5 | 1,27 |

Table B.1: Tabela $\eta \times \theta$

# Bibliography


[1] DØ Collaboration, S. Abachi *et. al.*, "Observation of the Top Quark", Fermilab - Pub - 95/028 - E (1995) submetido à Phys. Rev. Lett.

[2] CDF Collaboration, F. Abe *et. al.*, "Observation of the Top Quark in $p\bar{p}$ Collisions", Fermilab - Pub - 95/022 - E (1995) submetido à Phys. Rev. Lett.

[3] DØ Collaboration, S. Abachi *et. al.*, " The DØ Detector", Nucl. Instr. Meth. **A338**, 185 (1994).

[4] DØ Collaboration, S. Abachi *et. al.*, "Inclusive $\mu$ and $b$-Quark Production Cross Section in $p\bar{p}$ Collision at $\sqrt{s} = 1.8$ TeV", Phys. Rev. Lett. **74**, 3548 (1995)

[5] UA2 Collaboration, M. Banner *et. al.*, Phys. Lett. **B118**, 203 (1982).

[6] F. Halzen, A.D. Martin, "Quarks & Leptons: An Introductory Course in Modern Particle Physics", John Wiley & Sons, Inc (1984).

[7] V.D. Barger, R.J.N. Philips, "Collider Physics", Addison-Wesley Publishing Company (1987).

[8] C. Quigg, "Gauge Theories of the Strong, Weak, and Electromagnetic Interactions", Addison-Wesley Publishing Company (1983).

[9] R.P. Feynman, M. Gell-Mann, Phys. Rev. **109**, 193 (1958).

[10] R.P. Feynman, "The Theory of Fundamental Processes", The Benjamin/Cummings Publishing. Company (1961).

[11] R.P. Feynman, Phys. Lett. **23**, 1415 (1969).

[12] R.P. Feynman, "Photon-Hadron Interaction", The Benjamin/-Cummings Publishing. Company (1972)

[13] F. Halzen, P. Hoyer, Phys. Lett. **B154**, 324 (1985).

[14] P. Nason, S. Dawson and R.K. Ellis, Nucl. Phys. **B327**, 49 (1989).

[15] W. Beenakker, W.L. van Neerven, R. Meng, G.A. Schuler and J. Smith, Nucl. Phys. **B351**, 507 (1991).

[16] DØ Collaboration, S. Abachi *et. al.*, "A Study of the Strong Coupling Constant Using $W+$ Jets Processes", (1995), submetido à Phys. Rev. Lett.

[17] B.R. Webber,"QCD and Jets Physics", Cavendish–HEP–94/15, $27^{th}$ International Conference on High Energy Physics (proceedings), Glasgow, Scotland (1994).

[18] M. Schochet, "The Physics of Proton Antiproton Collisions", Lectures from Les Houches Summer School July - 1991, e FNAL-Conf-91/341-E.

[19] T. Huehn, Seminars about his Doctorate Thesis (1993).

[20] T. Sjöstrand, "Monte Carlo Event Generation for LHC", CERN-TH.6275/91

[21] F. Paige and S. Protopopescu, BNL Report no. BNL38034, 1986 (not published), versão 7.0.

[22] J.H. Cochran Jr., *Search for Truth in the eμ chanel at DØ*, Doctorate Thesis, State University of New York, Stony Brook (1993).

[23] J.D. Bjorken, "Particle Physics - Where do we go from here?", Beam Line, Vol. 22, 4 (1992).

[24] CTEQ Collaboration, J. Botts *et. al.*, Phys. Lett. **B304**, 159 (1993).

[25] C. Peterson, D. Schlatter, I. Schmitt, P.M. Zerwas, Phys. Rev. D **27**, 105 (1983);

[26] J. Chrin, Z. Phys. C **36**, 163 (1987)

[27] R.D. Field, R.P. Feynman, Nucl. Phys. **B136**, 1 (1978)

[28] R.D. Field, "Applications of Perturbative QCD", Addison-Wesley Publishing Company (1989).

[29] S. Squarcia, "Heavy Flavor Physics at LEP", CERN-PPE/94-69 (1994).

[30] UA1 Collaboration, C. Albajar *et. al.*, Phys. Lett. **B213**, 405 (1988); **B256**, 121 (1991).

[31] T. Huehn, *A Study of* $\pi/K \rightarrow \mu\nu$ *In-Flight Decay Backgrounds in the Central Region,* $|\eta| < 0.76$, DØ Note 1288. May 16, 1992.

[32] UA2 Collaboration, M. Banner *et. al.*, Phys. Lett. **B122**, 322 (1983).

[33] UA5 Collaboration, G.J. Alner *et. al.*, Nucl. Phys. **B258**, 505 (1985).

[34] J.G.R. Lima, "Estudo da Seção de Choque de Produção Inclusiva de Múons a Baixos Ângulos em Colisões $p\bar{p}$ a $\sqrt{s} = 1.8$ TeV", Doctorate Thesis, CBPF (1995).

[35] CDF Collaboration, F. Abe *et. al.* , Phys. Rev. Lett. **68**, 3403 (1992); **69**, 3704 (1992); **71**, 500, 2396, 2537 (1993); Phys. Rev. D **50**, 4252 (1994).

[36] S. Snyder, "The DØ Detector", DØ Note # 2500 (1995).

[37] C. Brown *et al.*, "DØMuon System With Proportional Drift Tube Chambers", Nucl. Instr. Meth. **A279**, 331 (1989).

[38] D. F. Anderson, H. K. Arvela, A. Breskin, G. Charpak, "A Simple "Vernier" Method for Improving the Accuracy of Coordinate Readout in Large Wire Chambers", Nucl. Instr. Meth. **224**, 315 (1984).

[39] D. Green, H. Haggerty, S. Hansen, M. Takasaki, "Accurate 2 Dimensional Drift Tube Readout Using Time Division and Vernier Pads", Nucl. Instr. Meth. **A256**, 305 (1987).

[40] DØ Collaboration, M. Fortner *et al.*, IEEE Trans. on Nucl. Science **38**, 480 (1991).

[41] PAW, the Complete Reference (1.07), CERN Program Library Q121 (1993).

[42] J. Linnemann, "Plotting and Fitting Binned Data", (não publicado) (1994).

[43] G.D. Lafferty, T.R. Wyatt, "Where to Stick Your Data Points: The Treatment of Measurements Within Wide Bins", CERN-PPE/94-72 (1994).

[44] V.D. Elvira *et al.*, "Smearing Correction to the Jet Cross Sections", DØ Note # 2247 (1994).

[45] G. D'Agostini, "A Multidimensional Unfolding Method Based on Bayes' Theorem", DESY 94-099, June 1994.

[46] DØ Collaboration, P. Quintas, "Measurement of $W$ and $Z$ Production Cross-Sections in $p\bar{p}$ Collisions at $\sqrt{s} = 1.8$ TeV," Proceedings of DPF 1994, and FNAL-Conf-94/341-E.

[47] Particle Data Group, L. Montanet *et al.*, "Review of Particle Properties", Phys. Rev. D **50**, 1173 (1994).

[48] OPAL Collaboration, R. Akers *et al.*, Z. Phys. C **60**, 199 (1993).

[49] A. Martin, R. Roberts, J.W. Stirling, Phys. Rev. D **47**, 867 (1993).